ANL-6474

ANL-6474

Argonne National Laboratory

RADIOLOGICAL PHYSICS DIVISION

SEMIANNUAL REPORT

July through December 1961

ANL-6474
Biology and Medicine
(TID-4500, 17th Ed.)
AEC Research and
Development Report

ARGONNE NATIONAL LABORATORY
9700 South Cass Avenue
Argonne, Illinois

RADIOLOGICAL PHYSICS DIVISION SEMIANNUAL REPORT

July through December 1961

J. E. Rose, Division Director
L. D. Marinelli, Associate Division Director

April 1962

Preceding Report:
ANL-6398 - January through June 1961

Operated by The University of Chicago
under
Contract W-31-109-eng-38
with the
United States Atomic Energy Commission

TABLE OF CONTENTS

TABLE OF CONTENTS

ULTRAVIOLET AND LIFETIME STUDIES OF MECHANISMS IN THE SCINTILLATION PROCESS*

I. B. Berlman

Abstract

The technique of using a pulsed beam of electrons to excite an organic scintillation solution and of recording the resultant pulse of emitted radiation is described. Sample pulse profiles and tabulated values of measured decay times of several solvents and solutes are presented.

For a paraxylene-diphenyloxazole (PPO) solution at low solute concentrations this technique was used to advantage to study the mechanism of nonradiative energy transfer from solvent to solute as a function of the solute concentration, and energy-transfer values were obtained which agreed favorably with those obtained by other coordinated methods. One such method, involving the static excitation of the solution by monochromatic uv radiation and the recording of the fluorescence spectrum, is described.

At high solute concentrations (PPO, ≥ 0.1 M), anomalies occur in the shape of the pulse contour and in the fluorescence spectrogram. This can be explained by assuming the formation of transient dimers. To the concept of the process leading to transient dimers, the postulate of a back reaction has been added.

*Presented at the 1961 International Conference on Luminescence, New York University, October 9-13, 1961 (to be published).

FLUORESCENCE QUENCHING OF A SCINTILLATING SOLUTION BY OXYGEN

T. Walter and I. B. Berlman

Several authors[1-5] have studied the quenching action of oxygen on a scintillation solution. A new and simple method is presented here for determining the rate constant for oxygen quenching of a solute in a cyclohexane solution. The results from this technique, moreoever, unequivocally reaffirm the assertion that solute quenching by oxygen is a diffusion controlled process.[6]

The technique of statically exciting an organic liquid solution by uv radiation and recording its fluorescence spectrum has already been described.[7] We recall that in the above reference it is also explained that, when the solute in a deaerated solution is excited directly, the intensity (L_0) of the emitted radiation is proportional to the quantum yield, $P_e/(P_e + P_i)$, when P_e is the probability per second for an excited solute molecule emitting its excess energy as radiation, and P_i is the probability per second for a nonradiative transition. The emission intensity (L) of the same solute in an aerated cyclohexane solution is proportional to $P_e/(P_e + P_i + P_q)$, where P_q is the probability per second for quenching of the excited solute molecule by oxygen. Therefore,

$$L_0/L = 1 + \frac{P_q}{P_e + P_i} = 1 + \tau P_q \quad , \qquad (1)$$

where $\tau = 1/(P_e + P_i)$ is the mean decay time of the solute in the absence of oxygen. Moreover, $P_q = k_q \cdot (c)$, where k_q is the rate constant for quenching of oxygen, and (c) is the concentration of dissolved oxygen in cyclohexane. Since cyclohexane is the common solvent, the concentration of oxygen is constant and the same for each solute when the solution is aerated.

In the present method the novelty in applying Equation (1) lies in plotting L_0/L versus τ, vis-a-vis the Stern-Volmer method[8] of plotting L_0/L versus (c).

The measured values of L_0/L and τ (in nsec) for several solutes are recorded in columns 3 and 4, respectively, of Table 1. These values are plotted in Figure 1, and it is noted that within the experimental limits all the points except those for m-terphenyl and naphthalene fall on a straight line. Since these supposedly nonconforming solutes have more than one decay component, it is not clear where they should be positioned on the τ axis.

Table 1

Fluor	Concentration (g/l)	L_0/L	τ (nsec)
1. PBD	?(<1)	1.06	2.4
2. PPO	1	1.11	2.7
3. α-NPO	1	1.12	2.8
4. p-terphenyl	1	1.10	2.7
5. anthracene	0.1	1.29	6.2
6. m-terphenyl	1	2.05	2.7 ~20.0
7. fluorene	1	1.54	11.2
8. diphenyl	1	1.96	19.0
9. naphthalene	1	7.2	90.0 >600.0
10. xylene*	-	2.4	27.0

*Xylene in a volume ratio of 10%.

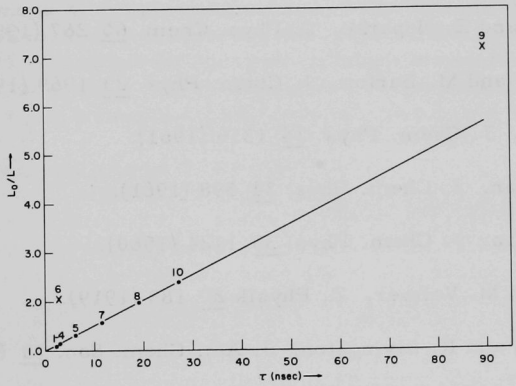

Figure 1

Plot of L_0/L versus the decay time τ of each solute, where L_0 is proportional to the quantum yield of the solute in a deaerated solution, and L is the same parameter for an aerated solution. The numbers refer to the solutes in Table 1.

From the slope of the straight line and the known value of (c) a value of $k_q = 2.3 \times 10^{10}$ liters/mole/sec is obtained. This value agrees very well with the diffusion constant for cylcohexane as computed from the formula, $k_q = 8\ RT/3\eta = 1.7 \times 10^{10}$ liter/mole/sec, where R is the gas constant, T is the absolute temperature, η is the viscosity in poise, and k_q is the rate constant for diffusion.[9] Thus we conclude that oxygen quenching in a cyclohexane solution is diffusion controlled.

We conclude that in the absence of decay-time apparatus, the value of τ of any solute in cyclohexane may be determined fairly accurately from a measurement of L_0/L and the application of the curve of Figure 1, provided that the solute has only one decay component.

References

1. R. W. Pringle, L. D. Black, B. L. Funt, and S. Sobering. Phys. Rev. 92 1582 (1953).

2. M. Furst and H. Kallmann. Phys. Rev. 97 583 (1955).

3. B. L. Funt and E. Neparko. J. Phys. Chem. 60 267 (1956).

4. P. J. Berry and M. Burton. J. Chem. Phys. 23 1969 (1955).

5. A. Weinreb. J. Chem. Phys. 34 1316 (1961).

6. I. B. Berlman. J. Chem. Phys. 34 598 (1961).

7. I. B. Berlman. J. Chem. Phys. 33 1124 (1960).

8. O. Stern and M. Volmer. Z. Physik 20 183 (1919).

9. E. J. Bowen and R. Livingston. J. Am. Chem. Soc. 76 6300 (1954).

AN ISOTOPE EFFECT IN THE PROBABILITY OF IONIZING A MOLECULE BY ENERGY TRANSFER FROM A METASTABLE NOBLE-GAS ATOM

William P. Jesse† and Robert L. Platzman

Excitation of a molecule to an electronic state lying above the ionization potential need not result in ionization. The excitation energy can be dissipated in a reorganization of the positions of the constituent atoms - by dissociation, predissociation, or internal conversion. This conclusion stems from the fact that the fraction of excitation acts leading to ionization, the "efficiency of ionization," $\eta(E)$, is almost always smaller than unity, at least when the excitation energy, E, is not more than 15-20 ev above the lowest ionization potential. Experimental values of $\eta(E)$ for diverse molecules have been obtained, both for excitation by absorption of a photon[1] (η_p) and for excitation by collision of the second kind with an excited atom[2] (η_c). No information is available for the equally interesting case of excitation by electron impact.

An important question which arises is whether there is true competition in the transient excited state between pre-ionization and atomic reorganization. This need not be the case: η might measure the probability of pathways that invariably lead to ionization, as opposed to pathways that invariably do not. In a simple model, with only two initial steps,

$$AB + \text{excitation energy } E \longrightarrow AB^+ + \epsilon^- \qquad [\underline{\text{direct}} \text{ ionization, probability } \delta]$$

or

$$AB + \text{excitation energy } E \longrightarrow AB^* \qquad [\text{excitation, probability } (1-\delta)],$$

the latter followed by

$$AB^* \begin{cases} \nearrow AB^+ + \epsilon^- & [\text{pre-ionization, rate } k_1] \quad (1) \\ \searrow A + B\ , & [\text{"atomic reorganization," rate } k_2], \quad (2) \end{cases}$$

it follows that

$$\eta = \delta + (1-\delta)k_1/(k_1+k_2) \quad . \qquad (3)$$

(Here AB denotes the molecule; neither A nor B need be monatomic.) Thus it is conceivable that $k_1 \ll k_2$ and hence $\eta \approx \delta$, in which case processes (1) and (2) would not be competitive.

---

†St. Procopius College, Lisle, Illinois

That the contrary is generally true is suggested strongly by arguments in a previous paper,[2] which concludes that, indeed, $\delta \ll 1$ is the typical behavior, and $\eta_c \approx \eta_p \approx 1/(1 + k_2/k_1)$ does measure a true competition.

Existence of competition in AB* can be tested by observing the effect on η of isotopic substitution in the molecule. Parameters determined by purely electronic reorganization - δ and k_1 - should thereby be unaffected. But k_2 will be diminished, and η therefore increased, if heavier masses are substituted; thus $k_2 = k_2' M^{-1/2}$, where M is an effective reduced mass for such atomic motions as bring the molecule to a point in coordinate space subsequent to which pre-ionization is impossible. This experiment has been performed. The predicted isotope effect is found, and in the anticipated sense: in every case the isotopic molecule with heavier atoms has a greater value of η_c. Hence pre-ionization and "atomic reorganization" are truly competitive.

Measurement of η_c is accomplished by observing the total ionization by high-energy particles in a noble gas contaminated with the molecule under study.[2,3] The ionization exceeds that in the pure noble gas if the latter's lowest excitation energy, E_0, exceeds the ionization potential, I_x, of the contaminant, chiefly because of ionization of the contaminant in collisions with metastable noble-gas atoms.[4,5] For all monatomic contaminants the augmentation is about the same, small differences between them arising from the effect of subexcitation electrons.[6] Molecular contaminants exhibit large differences in the collateral ionization, for η_c is peculiar to the individual contaminant molecule, and $0 \leq \eta_c \leq 1$. The value of η_c is given by $\eta_c \approx \Delta N_i / \Delta N_i^{at}$,[2] where ΔN_i is the augmentation observed (at the plateau, as in Figure 2), and ΔN_i^{at} is the augmentation expected if the contaminant were monatomic and had an ionization potential equal to $I_x (\Delta N_i^{at}/N_i \approx 0.395 + 0.34\,[1 - (I_x/E_0)]$, with $I_x < E_0$).

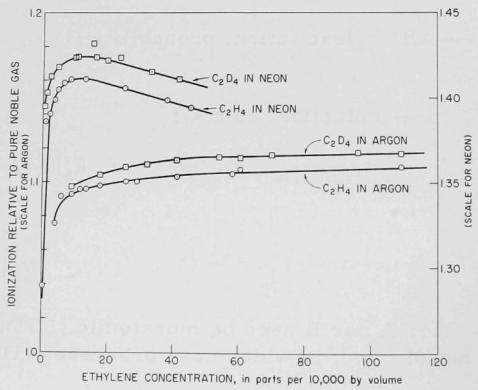

Figure 2

Ionization current in the mixture, relative to that in the pure gas, plotted against contaminant concentration, for normal and fully deuteriated ethylene in neon and in argon.

Ionization currents from beta rays (mean kinetic energy about 18 kev) of Ni^{63} deposited on a gridded electrode were determined in an ionization chamber by methods already described,[7] for various concentrations of the contaminant. Normal and fully deuteriated ethylene and n-butane were studied, both in neon and in argon. In Figure 2 the ionization in the mixture, relative always to the corresponding value, N_i, in the pure parent gas, is plotted against the measured concentration of contaminant introduced.

The curve for each deuteriated hydrocarbon is consistently higher than that for the corresponding normal one by the order of one per cent - about ten times the estimated error of measurement. In the plateau region the ratio of these ionizations, $(N_i + \Delta N_i^D)/(N_i + \Delta N_i^H)$, is found to be remarkably independent of contaminant concentration. Mean values for the four cases are presented in Table 2.

Table 2

Comparison of experimental and theoretical isotopic ionization ratios

Noble gas	Contaminant	Ionization ratio, $(N_i + \Delta N_i^D)/(N_i + \Delta N_i^H)$		Assumed splitting
		Experimental	Theoretical	
argon	ethylene	1.008_3	1.005 1.026	$CH_2 + CH_2$ $H + C_2H_3$
neon	ethylene	1.010_2	1.004 1.017	$CH_2 + CH_2$ $H + C_2H_3$
argon	n-butane	1.006_9	1.007 1.030	$C_2H_5 + C_2H_5$ $H + C_4H_9$
neon	n-butane	1.008_3	1.002 1.009	$C_2H_5 + C_2H_5$ $H + C_4H_9$

The magnitudes of the experimental results cannot be compared immediately with theory because none of the constants in Equation (3), δ, k_2'/k_1, and M, is known. However, assuming that $\delta \ll 1$, one can calculate the ionization ratio under specific assumptions regarding M. This is done in Table 2 for two extreme possibilities, symmetrical cleavage, and dissociation of an H atom. The calculated isotope effects are of the same order of magnitude as those observed; comparison suggests symmetrical splitting with Ar* ($\bar{E}$ = 11.6 ev), and dissociation of H (or H_2) with Ne* ($\bar{E}$ = 16.7 ev).

Additional conclusions are that pre-ionization in these highly excited states is slow, requiring times of the order of magnitude of 10^{-13} sec or longer; and that pre-ionization is not a rare phenomenon, but a prevalent one, since for most molecules the excited states with E somewhat greater than I possess a large part, and usually the greater part, of the total oscillator strength of the valence electrons.[2]

The results also point to the importance of similar experiments with absorption of light. It is predicted that the same isotope effect will be found in η_p.

We are indebted to Leon M. Dorfman (Argonne National Laboratory) for generously providing the deuteriated hydrocarbons, and to Ugo Fano (National Bureau of Standards) and Michel Magat (Sorbonne, Paris) for invaluable discussions.

References

1. G. L. Weissler. Handbuch der Physik. Berlin: Springer-Verlag, 1956. Vol. 21, p. 318.

2. R. L. Platzman. J. phys. radium 21 853 (1960).

3. R. L. Platzman. Intern. J. Appl. Radiation and Isotopes 10 116 (1961).

4. W. P. Jesse and J. Sadauskis. Phys. Rev. 88 417 (1952).

5. W. P. Jesse and J. Sadauskis. Phys. Rev. 100 1755 (1955).

6. R. L. Platzman. Radiation Research 2 1 (1955).

7. W. P. Jesse and J. Sadauskis. Phys. Rev. 97 1668 (1955).

LIQUID SCINTILLATOR SOLVENT STUDY FOR THE PURPOSE OF IMPROVING THE "TWIN" SCINTILLATION FAST NEUTRON DETECTOR. PART III

Roger Grismore and B. G. Oltman

The relative light yields of several more liquid scintillator solutions have been determined as a continuation of the program, described in previous reports,[1-3] which has the aim of improving the "twin" scintillation fast neutron detector.[4,5] As in the previous series[1,3] of measurements each solution consisted of 4 g/liter diphenyloxazole in the organic solvent under study. To prevent oxygen quenching of the scintillations each solvent was bubbled for 30 minutes with very pure nitrogen gas before insertion of the solute, and all operations incident to mixing solute and solvent and filling the cell were performed in the nitrogen atmosphere of a dry box.

The results of the present series of measurements are shown in Tables 3 and 4. The specimens of TS-28 and HF solvent reported on in Table 3 were laboratory samples donated by Arapahoe Chemicals, Inc., of Boulder, Colorado, and were used without further purification by us. The relative pulse heights from these solvents compared to that from paraxylene were determined under Co^{60} gamma irradiation in the manner outlined in our first report,[1] the pulse heights being measured to the peaks just below the Compton edges. In all the measurements presented in this paper the pulse heights have been normalized to a value of 163 paraxylene to permit direct comparison with our previous results.[1,3]

Table 3

Relative pulse heights from solutions of 4 g/liter diphenyloxazole in various organic solvents under Co^{60} gamma irradiation

Solvent	Grade	Ratio of number of protons to number of electrons	Pulse height at Compton peak, arbitrary units*
TS-28 (Shell Oil Co.)	Purified by Arapahoe Chemicals	0.169 ± 0.006**	122 ± 2
HF solvent (Arapahoe)	Scintillation	0.181 ± 0.006**	137.3 ± 1.4

*Pulse heights have been normalized to a value of 163 for the pulse height at the Compton peak of paraxylene.

**From chemical analysis.

Table 4

Pulse height from a solution of 4 g/liter diphenyloxazole in ethynylbenzene under Cs^{137} internal conversion electron irradiation

Solvent	Grade	Ratio of number of protons to number of electrons	Pulse height at point of inflection in electron peak, arbitrary units*
Ethynylbenzene	Distilled	0.111	20.1 ± 0.7

*Pulse height has been normalized to a value of 163 for the pulse height at the point of inflection in the electron peak of paraxylene.

The ethynylbenzene sample reported on in Table 4 was measured under internal conversion electron irradiation from Cs^{137} according to the method described in our last report.(3) In the case of the run on this solvent and in the corresponding run on paraxylene, pulse height was measured to the point of inflection in the high energy side of the electron peak owing to the fact that the peak was not too well resolved for ethynylbenzene. The latter solvent was freshly distilled just before measurement because it seems to turn yellow fairly quickly in storage.

The solvents TS-28 and HF are seen to be somewhat comparable to paraxylene in the properties pertinent to the "twin" scintillation detector and would be preferable for use in large volume cells because of their higher flash points. Ethynylbenzene is of particular interest because it contains only carbon and hydrogen and yet still has a relatively low proton-electron ratio. Thus, for high neutron energies it might be used as the hydrogen-deficient solvent in the "twin" scintillation detector in order to avoid the introduction of a third element such as fluorine with its attendant neutron-induced nuclear reactions.

References

1. Roger Grismore and B. G. Oltman. Argonne National Laboratory Radiological Physics Division Semiannual Report, July through December, 1960. ANL-6297, pp. 45-48.

2. L. D. Marinelli. Argonne National Laboratory Radiological Physics Division Semiannual Report, July through December, 1960. ANL-6297, pp. 49-54.

3. Roger Grismore. Argonne National Laboratory Radiological Physics Division Semiannual Report, January through June, 1961. ANL-6398, pp. 46-49.

4. I. B. Berlman and L. D. Marinelli. Rev. Sci. Instr. 27 858 (1956).

5. I. B. Berlman, R. Grismore, and B. G. Oltman. Rev. Sci. Instr. 31 1198 (1960).

SYSTEM FOR RECORDING PULSE SHAPES. PRELIMINARY REPORT

Orville J. Steingraber

Abstract

A new method of accurately recording scintillation pulse contours in the range of 10^{-9} sec is described. The excitation may be by pulsed uv, beta, or alpha sources.

Random pulses are sampled as to height by a standard pulse sampler.(1) Each pulse height sample is then converted to digital information and stored in the memory of a multichannel pulse-height analyzer. After a sufficient number of samples are taken to give a smooth curve, the information is plotted on an x-y recorder. The analyzer requires some modification as it is not used in the conventional manner.

Introduction

The method described aims to record and display the average pulse contour of several hundred randomly produced pulses of essentially equal shape but of not necessarily equal height. This allows the use of a reasonable band of energies from a given source of scintillator excitation without resorting to pulse height discrimination.

The oscilloscope uses the pulse sampling method to view the pulses. A simplified description is as follows: assume a pulse generator producing evenly spaced pulses 1,000 μsec apart (1 kc) and of a shape such as shown in Figure 3a. Each pulse presented to the oscilloscope is synchronized with a sampling pulse which is less than 0.5 nanoseconds wide. Each sampling pulse is progressively delayed 1 nsec with respect to the generator pulse (Figure 3b). The two pulses are summed, (Figure 3c) amplified, and stretched and presented to the vertical deflection of the oscilloscope. With proper Z axis blanking and an ordinary horizontal sawtooth deflection the information appears as dots of light on the screen. As can be seen, one horizontal sweep of a little more than 4,000 μsec represents about 5 nsec.

In actual practice, to preserve time linearity, the horizontal deflection is stepped in equal increments synchronously with the time of arrival of a trigger pulse which, in turn, forms the sample pulse.

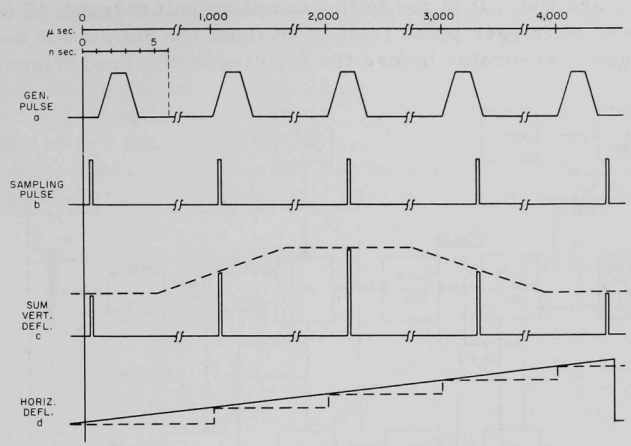

Figure 3

Pulse sampling technique (simplified).

Although the light level of the scintillations is relatively low, a small number of photomultiplier tube stages can be used because the input sensitivity of the sampling unit is only 10 mv. The use of a minimum number of stages aids in the preservation of the pulse rise time.

Because of the nature of the vertical deflection pulses which could be called amplitude modulated, each pulse is suitable to be converted to digital information and stored.

Apparatus

Briefly, the apparatus consists of a high-gain, fast-rise-time, (2 nsec), 14-stage photomultiplier tube and its 3,000-volt power supply. Only the first eight stages are needed to give sufficient gain. The output pulse of the photomultiplier tube is sampled by a type N plug-in unit in a Tektronics 531 oscilloscope. A proper trigger pulse for the sampler is provided by a Tektronics type 110 trigger regenerator. For analyzing, storing, and recording of the data, a RIDL 100 Channel Analyzer is used and its output plotted on an Electro-Instrument X-Y Recorder.

Operation

Figure 4 is a block diagram of the system. The negative output pulse of the photomultiplier tube is taken from the anode to which the last

six dynodes are tied. It is fed to the sampling unit through 40 feet of RG8/u cable. A trigger pulse is derived from the 8th dynode and amplified in the trigger regenerator before the forming of the final trigger pulse.*

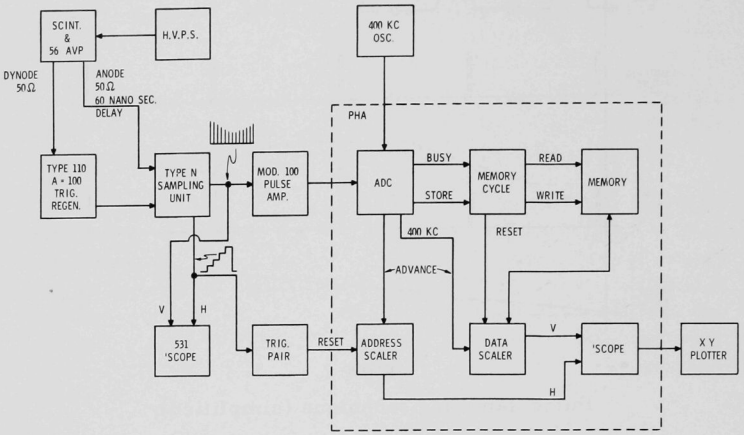

Figure 4

System block diagram.

Trigger pulses from the regenerator are fed to the horizontal input of the oscilloscope and to the sampling unit. Each pulse drives the horizontal sweep of the oscilloscope forward one step. The number of steps per sweep depends on the chosen number of samples (dots) per sweep. In this application it is adjusted to about 95 dots per sweep.**

In the sampling unit the trigger pulse also forms the very narrow sampling pulse. The incoming anode signal is added to this sampling pulse and the combined pulse amplified and stretched. A biased diode prevents passage of the signal pulse alone but will pass the peak of the sampling pulse or the sum of the two pulses. Successive samples are taken, each at a slightly later time in respect to the start of the anode pulse.

---

*The normal recovery time of 10 μsec of the trigger regenerator has been modified to about 500 μsec. This is done to allow storage of the sample pulse before the next sample is taken.

**The N unit has a 50, 100, 200, and 500 samples (dots) per display switch and an individual dots adjustment. The equivalent sweep speeds are 1, 2, 5, and 10 nsec per cm. The rise time of the unit is 0.6 nsec.

The sampling rate is, of course, dependent on the radiation source intensity and limited by the hold-off of the trigger regenerator.

A simplified diagram of the outputs of the sampling unit is shown in Figure 5. The vertical deflection pulses for the oscilloscope are about 2 μsec wide and are taken from the vertical output of the oscilloscope. With some differentiation and amplification they are suitable as an input to the analog-to-digital converter (ADC) of the pulse height analyzer.

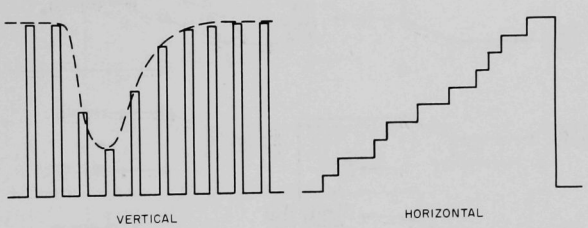

Figure 5

Sampling unit outputs (simplified)

Modification and Operation of the Analyzer

The analyzer is used as follows in the present system: (1) the address of an entry into the memory is determined by the time position of the sampling pulse relative to the sampled pulse, and (2) the number of pulses given to the data scaler for the entry corresponds to the amplitude of the sum of the sampling and signal pulses. The address scaler is cleared to zero for the first pulse sampled and then advances once for each successive one until 95 samples have been taken. Then the scaler is reset, and the pulse sampler starts sampling at the leading edge of the signal pulse again, and this cycle continues until 50,000 pulses have been sampled.

The analyzer may be modified so that it can be used in either this mode or the conventional mode by the addition of the switch shown in Figure 6. In the new mode the switch makes the following contacts:

Switch Section A. The normal address scaler reset pulse is switched to the address scaler input to advance the scaler once for each sample pulse.

Switch Sections B and F. The 2-mc pulse train from the ADC is switched to the data scaler input instead of the address scaler input. The frequency of the oscillator must be reduced to 400 kc, the maximum input rate of the data scaler.

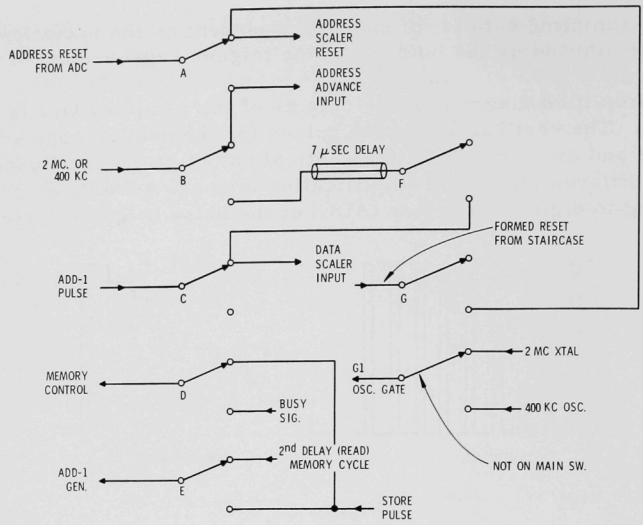

Figure 6

Analyzer switch (normal operating position) pulse routing.

Switch Section C. The data scaler ADD-1 input is opened and the delayed 400-kc pulse train is fed to the data scaler input.

Switch Section D. The ADC busy signal is used to initiate the memory store cycle, the first pulse of which is the data scaler reset, the second pulse the read pulse to the memory cores. After this time the memory cycle is stopped by Section E.

Switch Section E. The third pulse of the memory store cycle, ADD-1, is stopped by opening its input. At the end of conversion the normal store pulse is fed to the ADD-1 generator input which in turn drives the write pulse generator, completing the memory cycle.

Switch Section G. This supplies the address scaler reset pulse which is derived from the negative going edge of the horizontal staircase sawtooth voltage from the sampling unit.

Figure 7 shows the pulse timing of the store cycle when the previous modifications have been made.

The ramp voltage pulse in the ADC has been lengthened to approximately 0.1% per channel, referred to normal operation, because of the lower frequency, 400 kc, and to allow for sufficient vertical resolution.

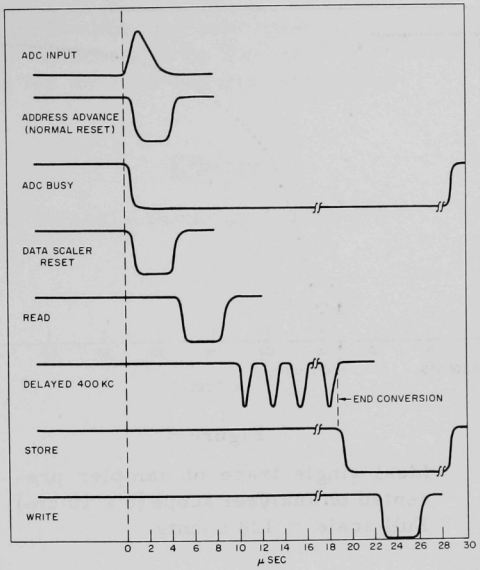

Figure 7

Store cycle timing of analyzer.

This allows approximately 130 cycles for a maximum amplitude pulse. Keeping within the limits then, 120 cycles x 2.5 μsec (400 kc) + 20 μsec of store time equals 320 μsec maximum time per sample pulse, hence, the necessity of the approximate 500 μsec hold-off of the trigger regenerator. The sampling rate then is limited to a maximum of 2000 per second with a high-intensity radiation source.*

If then the store rate is near the maximum and the base line adjusted to 120 counts per sample:

$$\frac{2{,}000 \text{ samples/sec}}{95 \text{ samples/sweep}} = 21 \text{ sweeps/sec} \quad .$$

This implies at 120 counts/sweep/sample a total of 2500 counts/sample/sec.

*Referring to Figure 8, the base line is adjusted by vertically positioning the sampling unit control while holding down the analyzer reset to zero. The pulse amplitude is adjusted by means of the photomultiplier tube high voltage and by inserting 50-ohm attenuators in the signal delay cable.

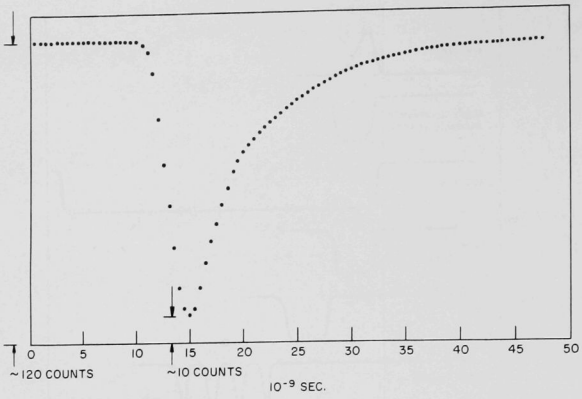

Figure 8

Ideal single trace of sampler presented on analyzer scope (6 x 10 cm). Full scale = 128 counts.

Similarly:

$$\frac{65{,}535 \text{ counts/sample (max storage)}}{2{,}500 \text{ counts/sample/sec}} = 26 \text{ sec to store}$$

This implies at 21 sweeps per second a total of 550 sweeps.

The process is completed by summing the individual sweeps of the sampling unit.

At present, the 2-nsec rise time of the photomultiplier tube has not been achieved with the present voltage divider arrangement. Although the sweep ranges of the sampling unit remain to be calibrated, some known decay times have been compared with success.

Some difficulty has been encountered in preventing reflections on the signal cable, possibly due to the trigger take-off on the 8th dynode, among other things.

With the exception of a slight base line slope in the sampling unit now being repaired, the system has operated successfully.

Thanks to I. B. Berlman for precipitating the idea and for his enthusiasm in the project. Thanks also to Warren L. Buck and Gene A. Mroz of the Physics Division for their advice and cooperation.

Reference

1. Robert Sugarman, Rev. Sci. Instr. 28 933 (1957).

SODIUM IODIDE SYSTEMS: OPTIMUM CRYSTAL DIMENSIONS AND ORIGIN OF BACKGROUND*

Harold A. May and Leonidas D. Marinelli

Abstract

The relatively high probability of gamma-ray interaction in sodium iodide, as well as its excellent spectrometric properties, are factors recommending its use in low-level in-vivo counting. To obtain maximum sensitivity consistent with economy, consideration must be given to the most efficient choice of crystal dimensions and to reduction of the background counting rate.

In order to gain some information on the economical utilization of crystal mass, a pilot study has been made for the case of point sources at distances of 40 cm. The method utilizes the photopeak fractions calculated by Miller and Snow for crystals of various sizes and gamma rays of various energies.(1) Results indicate an optimum thickness of about 2.5 cm at 300 kev, 5.0 cm at 700 kev and 10 cm from 1.5 to 3.0 Mev. Experimental results with the nonideal sources and detectors employed in actual practice will be discussed.

As to background in NaI crystals, studies have been in progress at this Laboratory since 1950, and early results were published in 1956.(2) Since then, more extensive and precise data have been gathered, aided greatly by the availability of large crystals and improved electronic instruments, which are necessary for whole body counting. Experiments to be described indicate that in a typical crystal and shield, the major sources of background pulses within the energy range from 25 kev to 1.6 Mev are as follows:

a) Shielding materials, 35 to 40% of total background
b) Cosmic rays, 24 to 28% of total background
c) Phototubes, 16 to 20% of total background.

The interpretation of coincidence pulse spectra extending to over 50 Mev obtained with plastic scintillator and GM tube anticonicidence shields in many different configurations has been greatly aided by comparison with similar spectra obtained with the same equipment located 76 meters underground. Typical spectra are discussed.

*Paper presented at I.A.E.A. Symposium on Whole Body Counting, Vienna, June, 1961.

In conjunction with current theories of deep penetration of gamma rays, a survey of the experimental performance of thick shields of materials of different atomic number has clarified the role played by the shield and suggested the feasibility of measuring very low specific gamma-ray activities of matter in bulk.[3]

References

1. W. F. Miller and W. Snow. Efficiencies and Photofractions for Sodium Iodide Crystals. Rev. Sci. Instr. 28 717 (1957); Energy Loss Spectra for Gamma Rays in NaI. Rev. Sci. Instr. 31 39 (1960).

2. C. E. Miller, L. D. Marinelli, R. E. Rowland and J. E. Rose. An Analysis of the Background Radiation Detected by NaI Crystals. IRE Trans. NS-3(4) 90 (1956).

3. L. D. Marinelli, C. E. Miller, H. A. May and J. E. Rose. Low Level Gamma-Ray Spectrometry: Experimental Requirements and Biomedical Applications. Advances in Biological and Medical Physics VIII. New York City: Academic Press (to be published).

Sr^{90}-Y^{90} BETA-RAY (AND BREMSSTRAHLUNG) DEPTH-DOSE MEASUREMENTS IN LUCITE*

Amrik S. Chhabra**

Abstract

In order to investigate the extent to which nuclear emulsions can be used in beta-ray dosimetry, depth-dose measurements of Sr^{90}-Y^{90} radiation in Lucite were first made by using a plastic scintillator (NE102) and a Failla extrapolation ion chamber down to and beyond the beta-ray range. Very good agreement was found between these methods throughout the region of beta-rays and bremsstrahlung. Measurements with NTB emulsion, however, proved to be grossly inadequate in regions where the absorbed dose is due mostly to bremsstrahlung. From the depth-dose measurements made with the scintillator, isodose curves were constructed for the particular applicator, covering a dose-rate range of 10^5.

*Accepted for publication in Radiology. This work was made possible through the financial support of International Cooperation Administration under Exchange Programme, and the laboratory facilities provided by the Radiological Physics Division of the Argonne National Laboratory.

**On leave from Atomic Energy Establishment, Trombay, Bombay, India

OPTIMUM CHOICE OF PARAMETERS IN ORDER TO DISTINGUISH BETWEEN LINEAR AND SQUARE DOSE-RESPONSE CURVES

John H. Marshall

Introduction

In order to determine whether the incidence of cancer in mice rises linearly or with the square of the absorbed radiation dose, one needs to know how many mice are required, what dose levels are optimal, and how the mice should be distributed among the various levels.

The choice of the square response as the alternative to linear has been made merely as one of the simpler possibilities. It need not imply a particular mechanism but may be regarded simply as a description of the slope of the dose-response curve on a log log plot in the given region of dose. Unless one chooses an alternative hypothesis, one cannot determine beforehand how many animals would be required to distinguish between linearity and nonlinearity with a given level of confidence.

In addition to the two hypotheses, one needs an estimate of the incidence at some (upper) dose level and an estimate of the control incidence. Then one can detetermine the optimum dose for one other (lower) dose level and the distribution of animals between the two levels and the controls. If the slope of the curve in more than one region is required, additional levels can be added, using as controls only those animals required by the lowest pair of dose levels.

Since it is the dose-dependent part of the incidence whose slope we wish to distinguish, we will subtract the control incidence from the incidence at each dose level before finding the dose dependence. The control incidence could be inferred, and the dose-response slope derived, from any three levels, but it involves less error, and therefore fewer animals, to measure the control incidence directly. Then it requires only two levels plus the controls to determine the dose dependence in a given region.

In the following calculations, tumor incidence refers to the total number of tumors divided by the number of animals at risk, and a Poisson distribution of the number of tumors has been assumed. The reason for these choices is given under Discussion below.

Calculation

1. Let the incidence (tumors per animal) at some given upper dose level be

$$I_1 = a + b$$

where

a = control incidence
b = incidence produced by given upper dose.

2. Then the incidence at some lower dose level will be, according to our hypotheses, either

$$I_2 = a + bx \quad \text{(Linear hypothesis)}$$

or

$$I_2 = a + bx^2 \quad \text{(Square hypothesis)}$$

where

$$x = \frac{\text{Lower dose}}{\text{Given dose}} \quad (0 < x < 1) \quad .$$

3. What we wish to discover, therefore, is whether the ratio

$$R \equiv \frac{I_2 - a}{I_1 - a} = x \text{ or } x^2 \quad .$$

4. To do this, we would like to reduce the standard error of R, $\epsilon(R)$, to a fraction of the difference between x and x^2 or

$$\epsilon(R) = \frac{x - x^2}{\eta} \quad .$$

There will be a somewhat different result depending on whether we use the linear or the square response to calculate $\epsilon(R)$, so both calculations will be made.

5. Now the standard error in R can be computed from the number of tumors which one would observe, on the average, given a certain number of animals

$$N = N_1 + N_2 + N_0$$

where

N_1 = the number of animals at the upper dose level

N_2 = the number of animals at the lower dose level

N_0 = the number of control animals.

6. The number of tumors at each level is then

$T_1 = N_1 (a + b)$

$T_2 = N_2 (a + bx)$ or $N_2 (a + bx^2)$

$T_0 = N_0 (a)$.

7. The standard deviations of these numbers, assuming a Poisson distribution, are then

$\epsilon(T_1) = \sqrt{N_1 (a + b)}$

$\epsilon(T_2) = \sqrt{N_2 (a + bx)}$ or $\sqrt{N_2 (a + bx^2)}$

$\epsilon(T_0) = \sqrt{N_0 a}$.

8. The standard deviations of the corresponding incidences are

$$\epsilon(I_1) = \frac{\epsilon(T_1)}{N_1} = \sqrt{\frac{a + b}{N_1}}$$

$$\epsilon(I_2) = \frac{\epsilon(T_2)}{N_2} = \sqrt{\frac{a + bx}{N_2}} \quad \text{or} \quad \sqrt{\frac{a + bx^2}{N_2}}$$

$$\epsilon(a) = \frac{\epsilon(T_0)}{N_0} = \sqrt{\frac{a}{N_0}} \quad .$$

9. The standard deviation of the numerator of R (Expression 3) is then

$$\epsilon(I_2 - a) = \sqrt{[\epsilon(I_2)]^2 + [\epsilon(a)]^2} = \sqrt{\frac{a + bx}{N_2} + \frac{a}{N_0}} \quad \text{or} \quad \sqrt{\frac{a + bx^2}{N_2} + \frac{a}{N_0}} \quad .$$

10. The standard deviation of the denominator of R is similarly

$$\epsilon(I_1 - a) = \sqrt{[\epsilon(I_1)]^2 + [\epsilon(a)]^2} = \sqrt{\frac{a + b}{N_1} + \frac{a}{N_0}} \quad .$$

11. Before calculating $\epsilon(R)$, we note that the control incidence contributions to the error of numerator and denominator (Expression 3) are not independent. In fact, they counteract each other to some extent. The total error in R contributed by any error in our knowledge of $\underline{a}$ is less than the error in R contributed by the error of $\underline{a}$ in the numerator alone. In other words, we are still slightly overestimating $\epsilon(R)$ if we simply neglect the last term in Expression 10 and set

$$\epsilon(I_1 - a) = \sqrt{\frac{a + b}{N_1}} \quad .$$

The effect of this approximation upon the results is small and on the safe side.

12. Then the standard error in R is R times the square root of the sum of the squares of the fractional standard deviations of numerator and denominator, or

$$\epsilon(R) = R \sqrt{\left(\frac{\epsilon(I_2 - a)}{I_2 - a}\right)^2 + \left(\frac{\epsilon(I_1 - a)}{I_1 - a}\right)^2} \quad .$$

13. For the linear hypothesis

$$\epsilon(R) = x \sqrt{\frac{1}{(bx)^2}\left(\frac{a + bx}{N_2} + \frac{a}{N_0}\right) + \frac{1}{b^2}\left(\frac{a + b}{N_1}\right)}$$

or

$$14. \qquad \epsilon(R) = \sqrt{\frac{a}{b^2}\left(\frac{1 + r\,x}{N_2} + \frac{1}{N_0} + \frac{x^2\,(1 + r)}{N_1}\right)}$$

where

$$r \equiv b/a$$

15. and for the square hypothesis

$$\epsilon(R) = x^2 \sqrt{\frac{1}{(bx^2)^2}\left(\frac{a + bx^2}{N_2} + \frac{a}{N_0}\right) + \frac{1}{b^2}\left(\frac{a + b}{N_1}\right)}$$

16. or

$$\epsilon(R) = \sqrt{\frac{a}{b^2}\left(\frac{1 + r\,x^2}{N_2} + \frac{1}{N_0} + \frac{x^4\,(1 + r)}{N_1}\right)}$$

where

$$r \equiv b/a \quad .$$

17. Now to find the optimum distribution of N animals among the groups N_0, N_1, and N_2, we wish to find the minimum of the bracket in Expression (14) or Expression (16) which in any case is of the form

$$F = \frac{A_0}{N_0} + \frac{A_1}{N_1} + \frac{A_2}{N_2}$$

when

$$N_0 + N_1 + N_2 = N$$

and the A's represent the corresponding numerators.

18. First, assume that one of the numbers, say N_1, is already the optimum value and determine the optimum value of N_0, considering N_0 and N_2 variables.

$$dF = -A_0 N_0^{-2} dN_0 - A_2 N_2^{-2} d N_2 = 0 \quad .$$

19. But $N_0 = (N - N_1) - N_2$

or

$$dN_0 = -d N_2$$

so

$$+ A_0 N_0^{-2} = + A_2 N_2^{-2}$$

or

$$\frac{N_2}{N_0} = \sqrt{\frac{A_2}{A_0}} \quad .$$

20. Any number could have been chosen as already optimum, so we have also that

$$\frac{N_1}{N_0} = \sqrt{\frac{A_1}{A_0}} \quad .$$

21. Then

$$N = N_0 + \sqrt{\frac{A_1}{A_0}}\, N_0 + \sqrt{\frac{A_2}{A_0}}\, N_0$$

or

$$N_0 = \frac{N}{1 + \sqrt{(A_1/A_0)} + \sqrt{(A_2/A_0)}} \quad .$$

22. Notice that $A_0 = 1$ in Expression (14) and Expression (16) so that the optimum numbers of animals are

(Figures 9 and 10)

$$N_0 = \left(\frac{1}{1 + \sqrt{A_1} + \sqrt{A_2}}\right)N$$

$$N_1 = \left(\frac{\sqrt{A_1}}{1 + \sqrt{A_1} + \sqrt{A_2}}\right)N \qquad \text{from Expression (20)}$$

$$N_2 = \left(\frac{\sqrt{A_2}}{1 + \sqrt{A_1} + \sqrt{A_2}}\right)N \qquad \text{from Expression (19)}$$

where

$$A_1 = x^2 (1 + r)$$
$$A_2 = 1 + rx$$

} Linear hypothesis

$$A_1 = x^4 (1 + r)$$
$$A_2 = 1 + r x^2$$

} Square hypothesis

23. Substituting these expressions for N_0, N_1 and N_2 into F Expression (17)

$$F = \left(\frac{1 + \sqrt{A_1} + \sqrt{A_2}}{N}\right)\left(1 + \frac{A_1}{\sqrt{A_1}} + \frac{A_2}{\sqrt{A_2}}\right)$$

or

$$F = \frac{\left(1 + \sqrt{A_1} + \sqrt{A_2}\right)^2}{N} \quad .$$

24. Therefore, on the linear hypothesis (substituting F from Expression (23) for the bracket in Expression (14)

$$\epsilon(R) = \frac{1 + x\sqrt{1 + r} + \sqrt{1 + rx}}{\sqrt{N}} \sqrt{\frac{a}{b^2}}$$

25. and on the square hypothesis [substituting F from Expression (23) for the bracket in Expression (16)]

$$\epsilon(R) = \frac{1 + x^2\sqrt{1 + r} + \sqrt{1 + r x^2}}{\sqrt{N}} \sqrt{\frac{a}{b^2}} \quad .$$

26. Combining Expression (24) and Expression (4) and solving for N

(Figure 11)
$$N = \frac{\eta^2 \left(1 + x\sqrt{1+r} + \sqrt{1+rx}\right)^2}{b\,r\,(x - x^2)^2}$$
(Linear hypothesis)

27. and combining Expression (25) and Expression (4) and solving for N

(Figure 12)
$$N = \frac{\eta^2 \left(1 + x^2\sqrt{1+r} + \sqrt{1+rx^2}\right)^2}{b\,r\,(x - x^2)^2}$$
(Square hypothesis)

These are the desired expressions for the total number of animals necessary to give η standard deviations between linear and square dose response curves where the parameters have been defined as in the table below.

Level	Dose	Number of animals	Tumors per animal	
			Linear	Square
Upper	1	N_1	$a + b$	$a + b$
Lower	x	N_2	$a + bx$	$a + bx^2$
Control	0	N_0	a	a
	Total	N		$r = \frac{b}{a}$

28. Expressions (26) and (27) are plotted in Figures 11 and 12 which show the product Nb as a function of x for different values of r. The optimum x can be chosen from these plots since it corresponds to minimum Nb. The optimum value of x approaches 0.45 as r becomes small.

29. In Figures 13 and 14, some of the information in Figures 11 and 12 has been replotted to show N as a function of $\underline{b}$ for different values of $\underline{a}$. The value x = 0.4 has been used since it is nearly optimum over the whole range. The effect of different x values upon N can be seen in Figures 11 and 12.

30. All these values of N assume that the optimum distribution of animals (Expression 22) has been used.

Discussion

The statistics of tumor experiments can probably best be described by a Poisson distribution because, volumetrically, the biological unit capable of forming a tumor is much smaller than a whole animal. Though

it is not known with certainty whether this unit is a part of a cell, a cell, a group of cells, or a part of a tissue, it is safe to assume that the number of such biological units is large and the probability of a tumor per unit is small, even when the number of animals is small and the incidence of tumors is large. Thus the number of trials, one of the parameters of the binomial distribution, is unspecifiable here except that it is certainly much larger than the number of animals. The Poisson distribution, together with the number of tumors, is probably more applicable than the binomial distribution because it requires only that the number of trials be large and probability of a tumor per trial small. (This point is somewhat academic, however, since the two distributions give practically the same results if the number of animals is greater than fifty and the incidence is less than ten percent.)

Therefore, it is a good approximation to compute the standard deviation of a tumor incidence measurement (at least that part of the actual standard deviation which arises from the statistics of small numbers) from the Poisson distribution, that is from the square root of the number of tumors observed, as in Expression (7).

The standard deviation of the ratio of two incidences corrected for the control incidence Expressions (8-12) has then been found using the rules for propagation of errors.[1] The error in this ratio has been slightly overestimated by the approximation in Expression (11). This makes N and N_0 a little too large, but it has the virtue that $N_0 \approx N_2$ as $r \to 0$.

All the foregoing is based on a given number of standard deviations η. If one assumes that the mean number of tumors in the population is large enough for their distribution in successive identical experiments to be approximately symmetrical about that mean, then one may infer what probability is associated with a given number of standard deviations by using the normal distribution. Let us assume that we have two normal distributions with the same standard deviation, their mean values separated by η times that standard deviation. The first represents the distribution of R values about the mean expected under the linear hypothesis, the second that under the square hypothesis (Expression 3). Figure 15 shows the probability that a value of R belonging to one of the distributions could mistakenly be assigned to the other under a given confidence requirement. This "chance of failure" in performing an experiment to distinguish the hypothetical possibilities is plotted versus η.

In Figures 11, 12, 13, and 14 we have taken $\eta = 3$, which corresponds to the vertical line in Figure 15. The effect upon the chance of failure of using different total numbers of animals, $N(\eta)$, is also shown, based on the number required for $\eta = 3$ and the fact that N is proportional

to η^2 (Expressions 26 and 27). Changing N and η does not change the optimum x or the optimum distribution of animals between the three levels.

When the number of tumors in the population is small, the normal distribution is no longer so good an approximation for the probability of a given deviation because the Poisson distribution is then asymmetrical. The probability of a given deviation below the mean is less than that above the mean. Therefore the square hypothesis calculation underestimates and the linear hypothesis calculation overestimates somewhat the number of animals required for a given error in Figure 15. The two calculations bracket the correct result. The average of the numbers of animals required by the two hypotheses in Figures 9, 10, 11 and 12 is probably fairly close to the truth.

The difference between the square and linear calculations for N is only partly to be explained by this Poisson asymmetry. Even an exact calculation shows that it is more difficult to prove that a square response is not linear than it is to prove that a linear response is not square. Suppose that 18 tumors are expected at the lower dose level under the linear hypothesis and only 9 tumors under the square hypothesis. The probability of observing 18 or more when 9 is the average number is 0.0053.(2) The probability of observing 9 or less when 18 is the average number is 0.0154.(2) Thus more animals would be required for a given accuracy in the latter case.

However, if for example the actual response is square, then the square calculation should be used to give the greatest chance that the data obtained will lie near the square values. Once the data are in, one must then turn around and calculate from the linear point of view the possibility that the data are really linear. Thus, in planning an experiment to distinguish the two hypotheses, both calculations must be taken into account. This provides a second reason for averaging the results of the two calculations.

Summary

To find the number of animals required to distinguish between a square and a linear dependence of incidence upon dose:

1. Estimate b and a.

2. Choose x in view of Figures 11 and 12. x = 0.4 is suggested as a useful compromise. The small values of x that are optimum for large values of b are probably not a wise choice when one considers that over such a wide dose range the type of response may be changing.

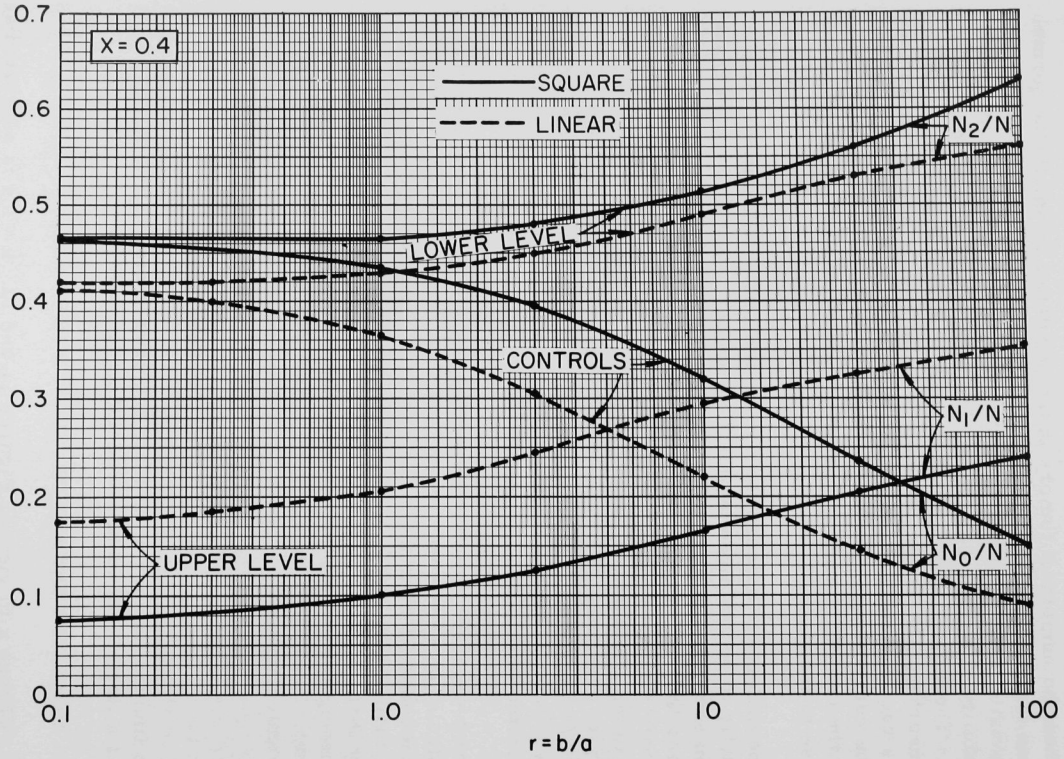

Figure 9

Optimum distribution of the animals between the two dose levels and the controls for x = 0.4. Curves for both the square and linear hypothesis are shown.

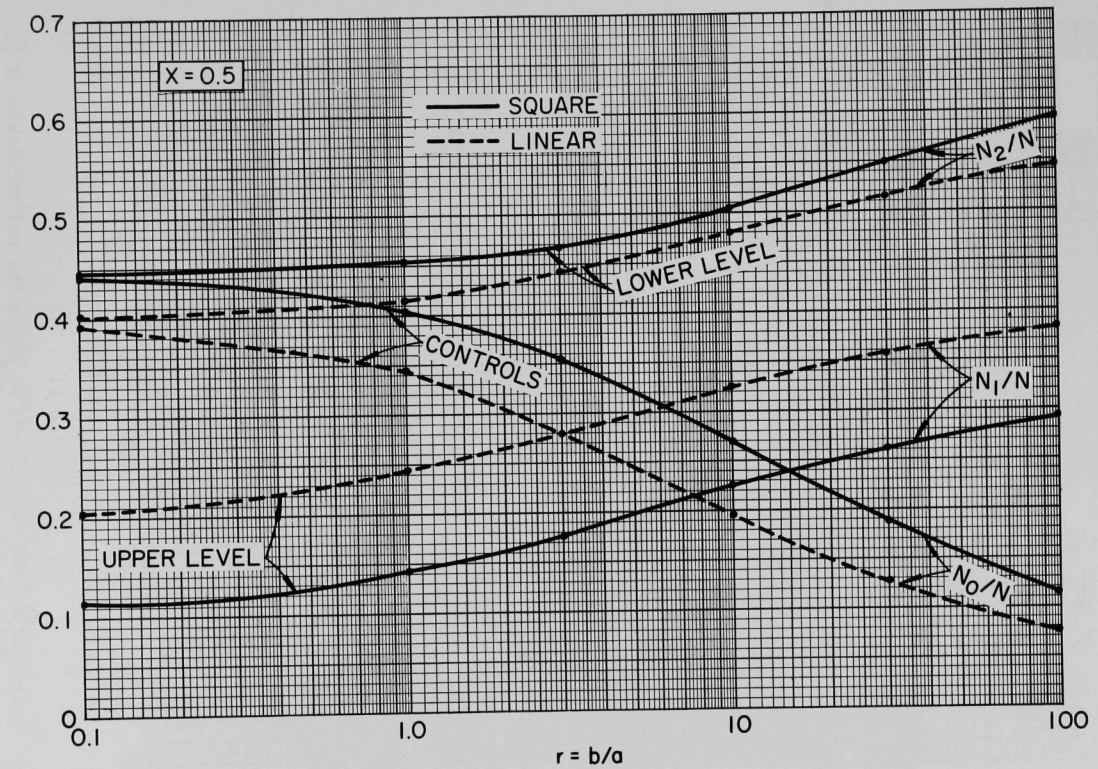

Figure 10

Optimum distribution of the animals between the two dose levels and the controls for x = 0.5. Curves for both the square and linear hypothesis are shown.

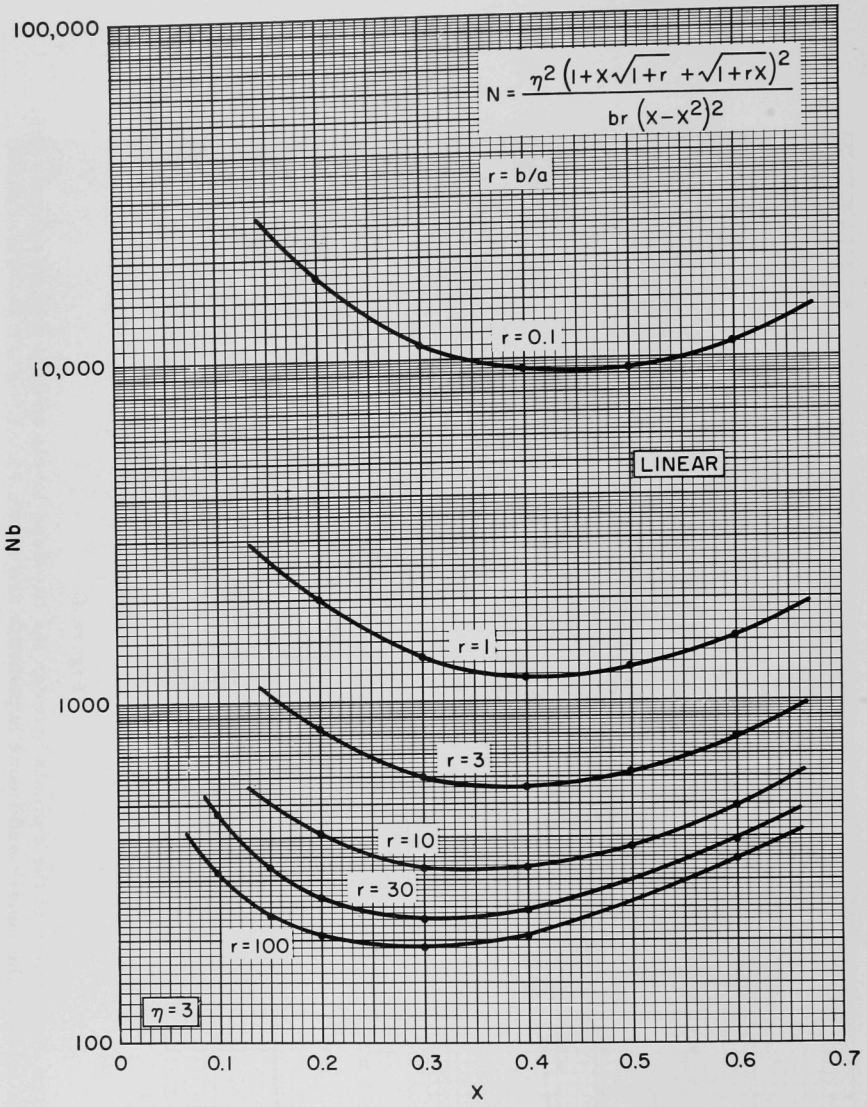

Figure 11

The total number of animals required, N, times the net incidence at the upper level, b, versus the ratio between the dose levels, x. Linear hypothesis, $\eta = 3$. (Optimum distribution of the N animals is assumed.)

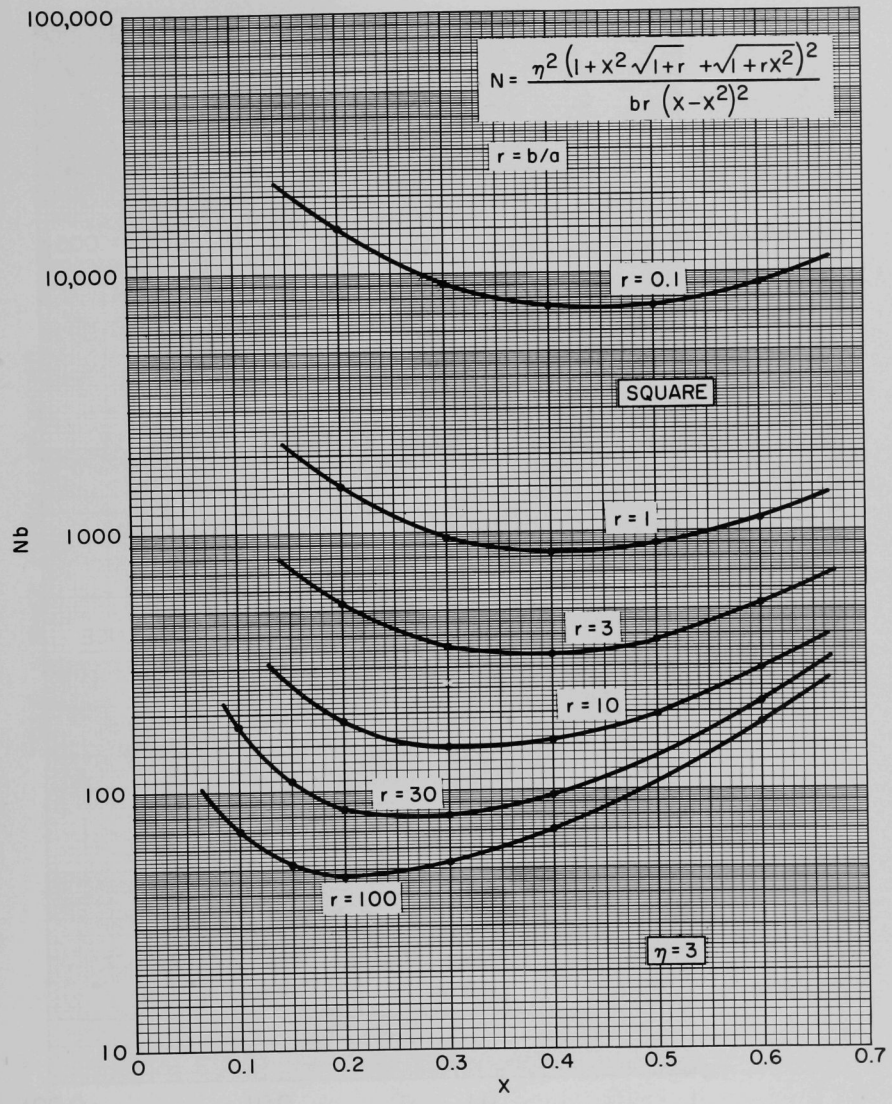

Figure 12

The total number of animals required, N, times the net incidence at the upper level, b, versus the ratio between the dose levels, x. Square hypothesis, $\eta = 3$. (Optimum distribution of the N animals is assumed.)

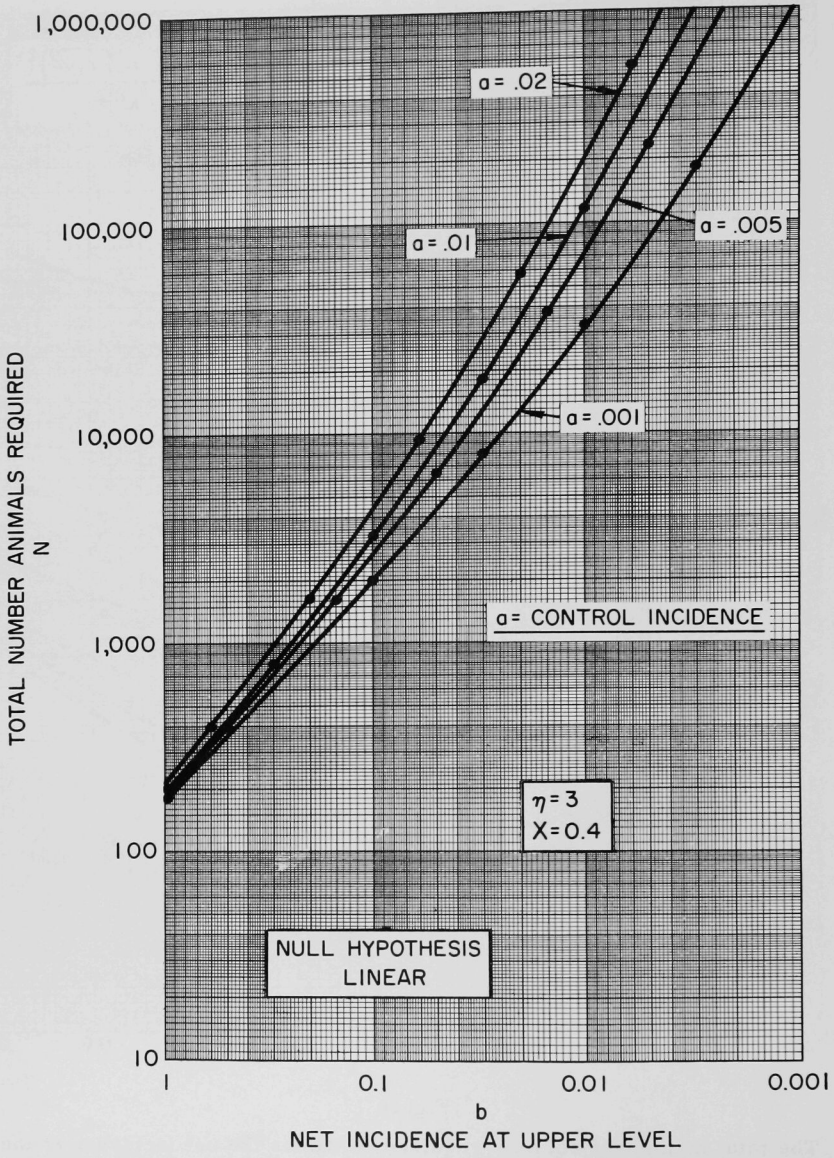

Figure 13

The total number of animals required, N, versus b for different control incidences, a, and for x = 0.4, η = 3. Linear hypothesis. (This figure is simply a replot of the information in Figure 11 for x = 0.4.)

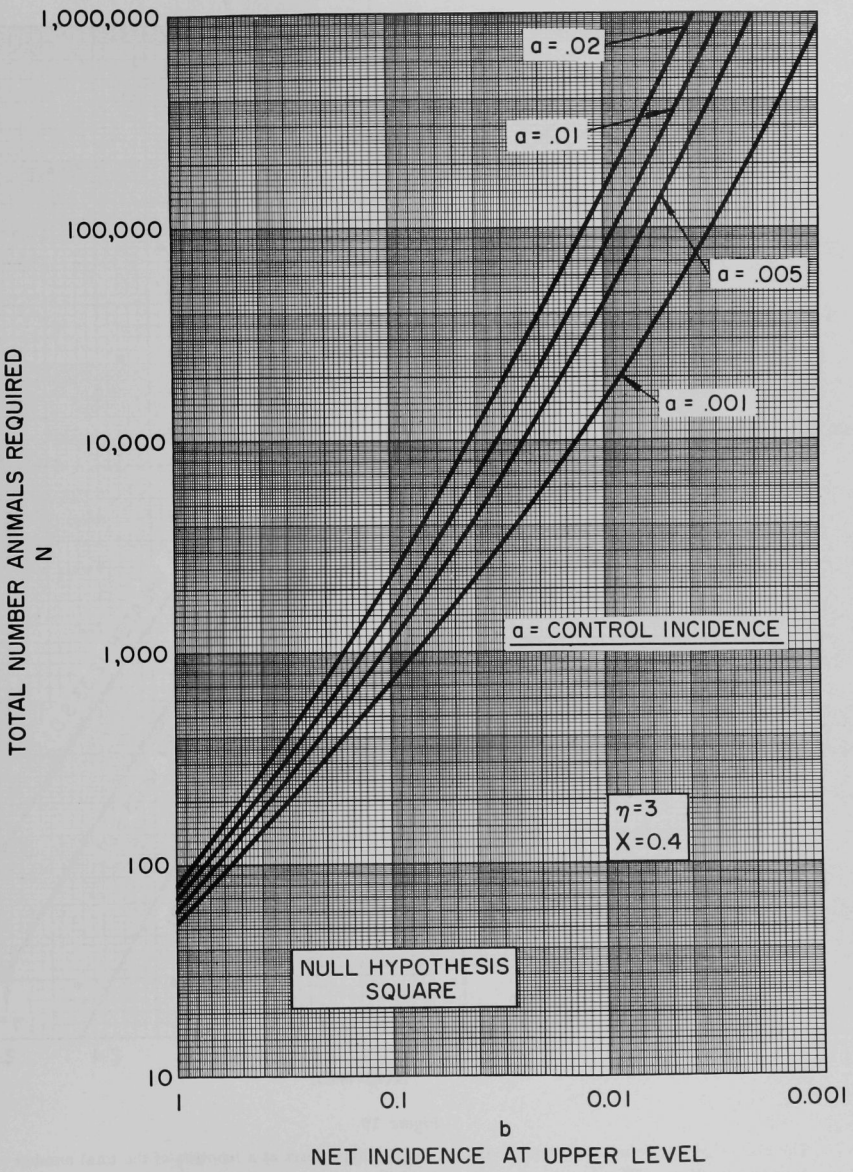

Figure 14

The total number of animals required, N, versus b for different control incidences, a, and for x = 0.4, η = 3. Square hypothesis. (This figure is simply a replot of the information in Figure 12 for x = 0.4).

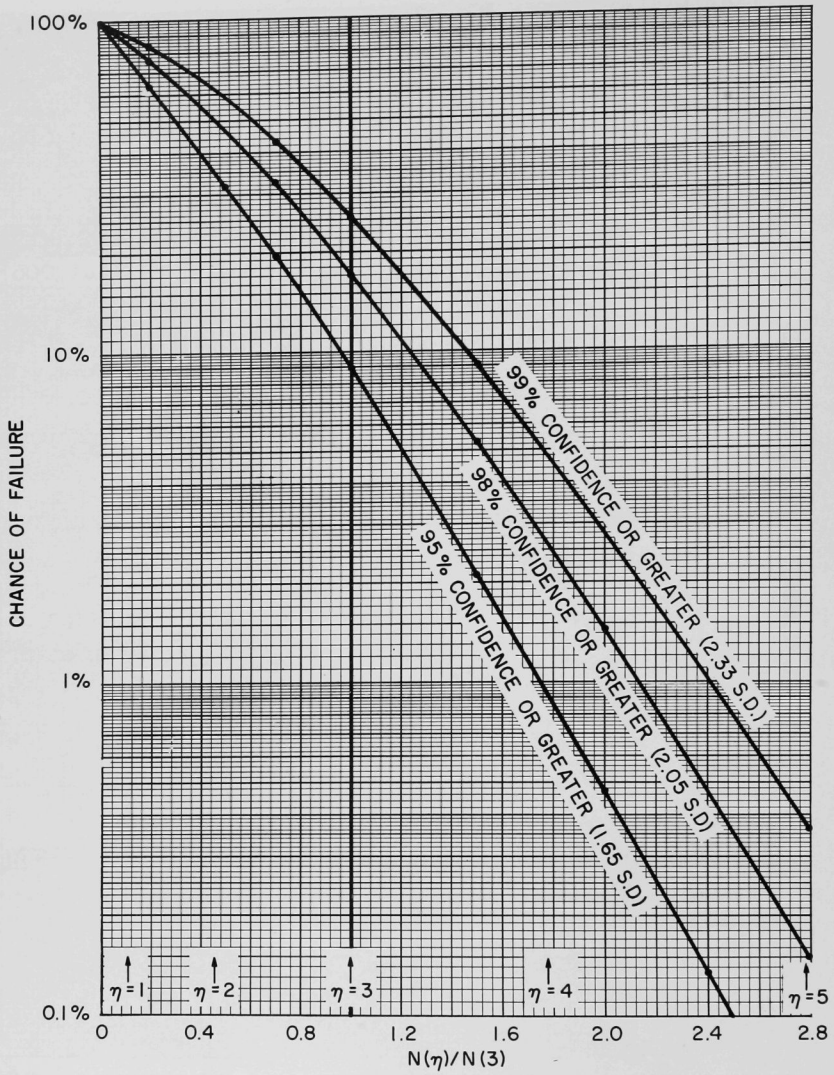

Figure 15

The chance of failure to discriminate between the two hypotheses as a function of the total number of animals used $N(\eta)$. The abscissa gives the ratio of the number of animals used to the number required for $\eta = 3$, the value of N given in Figures 11, 12, 13 and 14. Two normal distributions separated by η times their standard deviation have been assumed. These curves are approximately applicable here if the average of the N values for the two hypotheses (Figures 13 and 14) is used for N(3).

3. Read N in Figures 13 and 14 and take the average value. If you use an x value different from 0.4, correct the N values from Figures 13 and 14 by multiplying by the ratio of the corresponding Nb values for the nearest value of r in Figures 11 and 12 respectively.

4. Distribute the N animals among the three levels as shown in Figure 9 or 10 or Expression (21) (depending on which x value has been used), using the average of the square and linear results.

5. The total number of animals N may then be changed according to Figure 15 if $\eta = 3$ is not satisfactory. Such a change does not modify the other paramaters.

It is hoped that presenting the statistics of the problem in this form will help in planning experiments. It emphasizes the dependence of the results upon the input parameters, particularly upon b, the net incidence at the upper dose level. Though the results are approximations, the two calculations bracket the correct answer. Of course a different choice of hypotheses (such as linear versus threshold) will yield different results.

I would like to thank Sylvanus Tyler for helpful discussions.

References

1. R. D. Evans. The Atomic Nucleus. New York: McGraw Hill Book Co., Inc., 1955. p. 768.

2. E. C. Molina. Poisson's Experimental Binomial Limit (Tables). New York: D. Van Nostrand Co., 1947.

ACTIVATION ANALYSIS OF SOME HEAVY NUCLIDES

Richard B. Holtzman

Calculations were made to compare the sensitivities of neutron activation analysis with radiochemical and chemical techniques used for the determination of several naturally occurring radioactive nuclides present in the human environment, namely natural U, U^{235}, Th^{232}, Th^{230}, Th^{228}, Pa^{231}, Ac^{227}, Ra^{228} and Ra^{226}. All methods of analysis have limitations, and, in particular, human specimens are very limited in size. Bone samples, for example, usually range from 1/2 to 10 g. In the measurement of small amounts of material, reagents introduce contaminations of the order of magnitude of the quantities being measured. In some cases it may be very difficult to modify the procedure to handle larger samples. More significant is sample inhomogeneity. It is often desirable to study the smallest possible section, and bone, for example, is very obviously inhomogeneous, even on a macroscopic scale, with wide spatial variations of chemical composition. Modifications of present methods might improve in sensitivity by as much as an order of magnitude through the use of counters of reduced backgrounds and improved electronic stability, but this involves extremely long counting times which would tie up special equipment for long periods of time for each sample measured.

Chemical methods of analysis, such as spectrophotometry, are limited to the determination of microgram quantities. Fluorimetric methods may be used to determine as little as 10^{-10} g of U[1] and 10^{-8} g of Th[2] although here one is also limited by reagent contamination. X-ray fluorescence in conjunction with an electron probe can measure 10^{-14} g of a particular element in a surface as small as one square micron, but measurements of these elements are limited to those in concentrations of the order of 0.1%.[3]

Neutron activation analysis, when applicable, may improve sensitivities by several orders of magnitude. With sensitivities such that milligram rather than gram samples could be analyzed, it would be possible to make microdistribution studies to a certain extent and even to analyze biopsy samples for particular radionuclides. Activation analysis often permits the analysis of several nuclides since the separation procedures are usually not as delicate as those of chemical separations in which it is usually only possible to extract one nuclide. A major advantage is that the reagent contamination may be eliminated as a source of error by irradiating the sample after a minimum of processing. None of the nuclide of interest is added to the sample until after irradiation; then the reaction product, rather than the reactant, becomes the object of interest. Neutron activation analysis has the disadvantage that a nuclear reactor is necessary for highest flux (and sensitivity). Fairly intense radiations are involved, and not all nuclides and

their reaction products are satisfactory for this procedure. Moreover, secondary reaction products may interfere with the analyses. In the main, this method is satisfactory, mainly, when the other procedures are unsuitable.

Thermal neutron activation rather than activation in general is discussed because of the high fluxes available in reactors along with high absorption cross sections for neutrons, particularly thermal neutrons, compared to those available in particle accelerators. In general, only thermal neutrons are used because these generally constitute a large fraction of the total neutron flux; even most of the superthermal neutrons are mainly in the ev energy region rather than in the Mev region necessary to produce nuclear reactions other than (n,γ).

The absorption cross sections are higher for the thermal and epithermal neutrons. Reactions other than (n,γ), such as fission, are possible, but few nuclei of interest fission under thermal neutron bombardment. Even when fission is a possible process, it is often not a desirable one to use since several nuclides in the sample may be fissionable under the irradiation conditions, and the nature of the fission products is not specifically dependent on the parent nuclide. Fission may be used where the combination of concentration and cross section of the nuclide of interest is such that the fission yields from this nuclide are much greater than those from the other nuclides. The parent nuclides may also be separated before irradiation, but one again encounters the problem of reagent contamination.

It is possible to use 14-Mev neutrons. Fluxes at this energy are of the order of 10^{-3} to 10^{-4} times those of the slow neutron fluxes available in reactors; and the cross sections for the reactions, such as (n, 2n), are 1/10 to 1/100 the reactor neutron cross sections for (n,γ) reactions.(4-8)

Charged particle reactions, such as (p,n), (p,f), (d,γ) and (α,n) in the energy region up to about 30 Mev have yields comparable to present-day (n,γ) reactions. The cross sections are in the tens of millibarns range as illustrated in Table 5, but currents of the order of 100 microamperes (6×10^{14} particles sec^{-1}) are available. If sensitivity of the method is represented by the cross section-flux product, one obtains 6×10^{12} for charged particles (σ = 10 mbarn, current = 100 μa) compared to 10^{14} for neutrons (σ = 10 barns, flux = 10^{13} neutrons sec^{-1} cm^{-2}). Variations in cross sections could equalize these figures. These methods could be limited by secondary reactions or reactions from other nuclides. These interferences are more likely to occur in charged-particle reactions in which high energies are available for the production of interfering reactions. Neutron energies go up to about 12 Mev in a reactor, but above the thermal region, the number in a given energy range drops off rapidly with energy so that neutrons of energy high enough to induce reactions other than (n,γ) are a relatively small contaminant. In addition, not all types of samples

are usable in an accelerator because of the high temperatures produced by the beam; a 100 μa beam of 10 Mev particles produces 1000 watts. At extremely low concentrations, recoil of the product nucleus from the container into the sample may be a significant contaminant, particularly when a particle is emitted.

Table 5

Cross sections for some nuclear reactions

Nuclear reaction and energy of bombarding particle	Th^{232} barns	Ra^{226} barns	U^{238} barns
(n,γ)[9] thermal	7.5	20	2.8
(n,γ)[5] 14 Mev	$\sim 5 \times 10^{-3}$	$\sim 5 \times 10^{-3}$	$\sim 5 \times 10^{-3}$
(n,2n) 14 Mev	0.65[10]	1.6[6]	
(n,3n)[6] 14 Mev		0.63	
(n,f)[11] 23 Mev		37×10^{-3}	
(n,f)[7] 14 Mev	0.37		2.3
(n,p)[8] 14 Mev	$\sim 1 \times 10^{-3}$	$\sim 1 \times 10^{-3}$	
(n,α)[8] 14 Mev	$\sim 1 \times 10^{-3}$	$\sim 1 \times 10^{-3}$	
(d,γ)[12] 15-20 Mev			1×10^{-3}
(p,f)[13] 11 Mev		$\sim 2\text{-}4 \times 10^{-3}$	

For purposes of calculation, consideration will be given only to neutron activation of the nuclides in which the activation product is chemically separated and determined by α- or β- counting. The sensitivities of the counters for detection of the activation products will be assumed to be about equal to the background counting rates of the counters available in this laboratory, (0.040 dpm for alpha emitters and 0.2 dpm for beta emitters). The disintegration of only one nuclide in a radioactive series

will be considered since the statistical errors depend mainly on those resulting from the counting of the parent nuclide, and we are only interested in the order of magnitude of the sensitivities.

Two experimental situations will be assumed: one, a present-day practicality in which fluxes of 10^{13} neutrons sec^{-1} cm^{-2} are available, such as in CP-5; the other, a likely future possibility in which 10^{16} neutrons sec^{-1} cm^{-2} will probably be available in five years or so.

The activity produced is calculated from the equation

$$A = f\sigma n (1 - e^{-\lambda t})$$

where

A is the activity of the activation product at the end of the irradiation,
f is the neutron flux in neutrons sec^{-1} cm^{-2},
σ is the neutron absorption cross section,
n is the number of atoms of the nuclide being determined,
λ is the decay constant of the activation product, and
t is the time of irradiation.

The sensitivity based on the counting sensitivities is

$$N = \frac{A\ (A.W.)}{f\ (1 - e^{-\lambda t}) \times 60 \times 6.023 \times 10^{23}}$$

where

N is the minimum detectable weight of the nuclide of interest,
A.W. is the atomic weight of the nuclide of interest,
6.023×10^{23} is Avogadro's number and the factor 60 is to convert A from dps to dpm, since f is given in units of neutrons sec^{-1} cm^{-2}.

The nuclides of interest in the study of naturally occurring materials in biological systems are natural uranium (U^{238} in radioactive equilibrium with U^{234} and with 0.75% U^{235}), enriched U^{235}, Th^{232}, Th^{230}, Th^{228}, Pa^{231}, Ac^{227}, Ra^{228} and Ra^{226}. U and Th may be determined fluorimetrically with high sensitivity, 10^{-10} and 10^{-8} g, respectively. Radiochemical techniques, that is separation and counting of the natural disintegrations of the nuclides of interest, may also be used. The sensitivity in terms of weight, depends, by this method, on the specific activity of the nuclide - that is, inversely on the half-life. As shown in Table 6, the radiochemical method for natural U and Th^{232} is less sensitive than the chemical method. The radiochemical and chemical methods are about equally sensitive for enriched U^{235}; however, in actual practice the radiochemical method is more sensitive by an order of magnitude because U^{234}, which has a high specific activity, is separated along with the U^{235} during the enrichment process. The sensitivities of the chemical and radiochemical methods are shown in Table 6.

Table 6

Sensitivities of various methods of analysis (chemical, radiochemical and neutron activation)

Element or nuclide	Sensitivity					
	Chemical, g	Radiochemical		Activation (saturation or 1 month)		
		p Curies*	g	Reaction	g**	g†
U(natural) (U^{238}, U^{234}, U^{235})	10^{-10}	0.018	3×10^{-8}	(n,γ)	4.7×10^{-14}	4.7×10^{-17}
				U^{238}(n,f) U^{235}(n,f)	1.2×10^{-14}	1.2×10^{-17}
U^{235}	10^{-10}	0.018	8×10^{-9}	(n,f)	2×10^{-15}	2×10^{-18}
Th^{232}	10^{-8}	0.018	1.6×10^{-7}	(n,γ)	1.7×10^{-14}	1.7×10^{-17}
Th^{230}	10^{-8}	0.018	9.2×10^{-13}	(n,γ)	3.7×10^{-15}	3.7×10^{-18}
Th^{228}	10^{-8}	0.018	2.2×10^{-17}	-	-	-
Pa^{231}		0.018	4×10^{-13}	(n,γ)	6.3×10^{-16}	6.3×10^{-19}
Ac^{227}		0.090	1.2×10^{-15} (β) 2.5×10^{-17} (α)	(n,γ)	2.5×10^{-16}	2.5×10^{-19}
Ra^{228}		0.090	3.3×10^{-16}	(n,γ)	3.5×10^{-15}	3.5×10^{-18}
Ra^{226}		0.018	5×10^{-15}	Ra^{226}(n,γ)Ra^{227}	6.2×10^{-15}	6.2×10^{-18} (β counting)
				$Ra^{227} \rightarrow Ac^{227}$	1.3×10^{-15}	1.3×10^{-18} (α counting, irradiated to saturation)
				$Ra^{227} \rightarrow Ac^{227}$	5×10^{-13}	5×10^{-13} (α counting month irradiation)

*p = pico (10^{-12})
**flux = 10^{13} n cm^{-2} sec^{-1}
†flux = 10^{16} n cm^{-2} sec^{-1}

Table 7 shows the reactions obtained in slow neutron activation and the subsequent decay chains of interest. In order to be useful, the cross section for neutron activation must be greater than 0.1 barn and the decay chain of the activation product and its daughters should have half-lives of at least a few minutes but not more than a few weeks. At least one nuclide must decay by a useful radiation, an alpha or beta of reasonable energy. Gamma rays are useful, but because of the high background count rates of efficient gamma detectors, the sensitivities are greatly reduced. Except for Ra^{226}, fewer than two useful decays occur in the activation product chain because of a long-lived daughter which breaks the chain. No useful daughters occur in the U^{235} and Th^{228} activation chain. However, slow neutron fission of U^{235} may be used for analysis.

Natural uranium may be irradiated for an hour or so, the uranium separated from the sample and the 23.5-min U^{239} counted. For small amounts of uranium this method is not accurate because of the few total counts observed. However, if the sample is irradiated several days, the 2.3-day Np^{239} may be separated and counted to give a higher total count. Because of the natural content of U^{235}, its fission products may be separated.

The thermal neutron cross section for fission of natural U is about 4.5 barns. In terms of detectability, the over-all cross section for this process is somewhat less than 0.5 barn, the fission yield being less than 10% for any given fission product which might be separated. The presence of fast neutrons in the high flux regions of a reactor would enhance the effective fission cross section because of the fast neutron fissioning of U^{238}.

Table 7

Element or nuclide	σ (for reaction), barns	Nuclear reactions[14]
U(natural (U^{238}, U^{235}, U^{234})	2.8	$U^{238}(n,\gamma)\ U^{239} \xrightarrow[1.2\beta^-]{23.5m} Np^{239} \xrightarrow[0.33\text{-}0.72\beta^-]{2.3d} Pu^{239} \xrightarrow{2.43 \times 10^4 y}$
	2.3	$U^{238}(n_{fast},f)$ Fission products
	0.8	$U^{235}(n,\gamma)\ U^{236} \xrightarrow{2.39 \times 10^7 y}$
	4.4	$U^{235}(n,f)$ Fission products
U^{235}	108	$U^{235}(n,\gamma)\ U^{236} \xrightarrow{2.39 \times 10^7 y}$
	590	$U^{235}(n,f)$ Fission products
Th^{232}	7.5	$Th^{232}(n,\gamma)\ Th^{233} \xrightarrow[1.2\beta^-]{23.3m} Pa^{233} \xrightarrow[0.26\beta^-]{27.4d} U^{233} \xrightarrow{1.6 \times 10^5 y}$
Th^{230}	35	$Th^{230}(n,\gamma)\ Th^{231} \xrightarrow[0.09\text{-}0.299\beta^-]{25.6h} Pa^{231} \xrightarrow{3.4 \times 10^4 y}$
Th^{228}	120	$Th^{228}(n,\gamma)\ Th^{229} \xrightarrow{7300\ y}$
Pa^{231}	200	$Pa^{231}(n,\gamma)\ Pa^{232} \xrightarrow[0.28\text{-}1.24\beta]{1.31d} U^{232} \xrightarrow{74\ y}$
Ac^{227}	520	$Ac^{227}(n,\gamma)\ Ac^{228} \xrightarrow[1.1\beta^-]{6.13h} Th^{228} \xrightarrow{1.9y}$
Ra^{228}	36	$Ra^{228}(n,\gamma)\ Ra^{229} \xrightarrow[\beta^-]{5m} Ac^{229} \xrightarrow[1.2\beta^-]{66m} Th^{229} \xrightarrow{7300y}$
Ra^{226}	20	$Ra^{226}(n,\gamma)\ Ra^{227} \xrightarrow[1.3\beta^-]{41m} Ac^{227} \xrightarrow[0.049\beta^-]{22y} Th^{227} \xrightarrow[5.4\alpha]{18.2d} Ra^{223} \xrightarrow[5.7\alpha]{11.6d}$
		$Em^{219} \xrightarrow[6.8\alpha]{3.92s} Po^{215} \xrightarrow[7.36\alpha]{0.0018s} Pb^{211} \xrightarrow[1.4\beta]{36.1m} Bi^{211} \xrightarrow[\beta^-]{2.15m} Po^{211} \xrightarrow[7.43\alpha]{0.52s}$
		Pb^{207} (stable)

Th^{232} may be determined by irradiating a short time and then separating and counting the 23-min Th^{233}; or a more accurate determination may be made by a long irradiation with separation and counting of the 27.4-day Pa^{233} daughter of Th^{233}.

Th^{230} has only one useful activation product, as does Pa^{231}. Ac^{227} may be determined from the 6.1-hr Ac^{228}. This however implies the absence of Ra^{228} which would also produce Ac^{228} in the course of its natural radioactive decay.

Ra^{228} may be determined by irradiating for several hours and separating and counting the 66-min Ac^{229}. This method is useful only where very rapid analysis is possible because the 6.13-hr Ac^{228} daughter of Ra^{228} will be present to mask the Ac^{229}.

Ra^{226} may be determined from the decay of the 41-min Ra^{227}. On the other hand, if the long-lived 22-yr Ac^{227} is used, the sensitivity may be improved up to a factor of 5 in addition to obtaining more total counts. The sensitivities attainable with various irradiation conditions are shown in Figure 16 in which the sensitivity in g Ra^{226} is plotted against irradiation time up to about 4 years. The radiochemical sensitivities of the present methods are also plotted for 2 scales, 10^{13} and 10^{16} neutrons sec^{-1} cm^{-2} (n = 13 and n = 16).

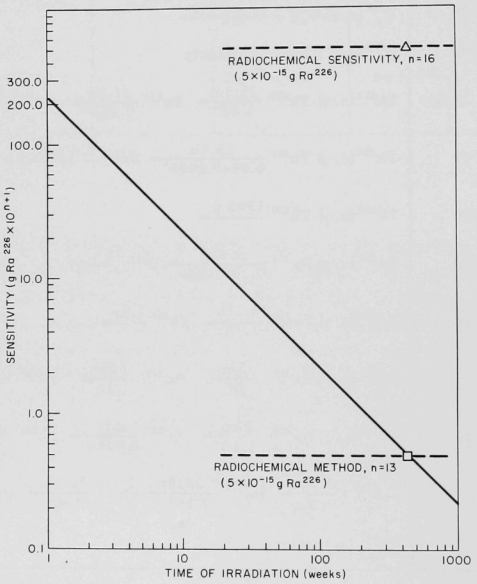

Figure 16

Sensitivity of neutron activation and radiochemical methods for the analysis of Ra^{226} (n is the $\log_{10}$ of the neutrons cm^{-2} sec^{-1} in the reactor).

One must be careful in using the results obtained here for activation analysis because they represent the limits of sensitivity; under actual conditions the sensitivities may be an order of magnitude lower when one considers chemical yields, decontamination problems, and the extremely low limits of the counting rates taken for these calculations. At extremely high sensitivities, contamination of the sample by the container may become an important problem. However, the sensitivities derived here may actually be feasible since reactors, producing 10^{14} neutron sec^{-1} cm^{-2}, such as the MTR, are available at the present time.

Even with the problems discussed above, neutron activation would be useful for the analysis of natural and enriched U and for Th^{230}, Th^{232}, and Pa^{231} with the present day neutron fluxes of about 10^{13} neutrons sec^{-1} cm^{-2}. Sensitivity improvements of 10 to 10^5 over other methods are possible and have actually been used to determine U and Th^{232}.

Radiochemical techniques are superior for the analysis of Ac^{227} and even with neutron fluxes of 10^{16} neutrons sec^{-1} cm^{-2} only a moderate improvement with neutron activation is likely.

As Table 6 shows, the present methods for the determination of Ra^{228} are superior by a factor of 10 to what is possible by activation with a 10^{13} neutron sec^{-1} cm^{-2} flux. With the higher flux, the activation appears to be about 100 times more sensitive. However, a practical improvement of 10 is more reasonable. In addition, the relatively short half-life of the Ac^{229} would mean that not only would activity be lost during the processing time of at least 1 hour, but the total number of counts would be small compared to that observable from the present method of separating and counting the 6.13-hr Ac^{228}. Consequently, neutron activation for the determination of Ra^{228} appears to offer little advantage over the present radiochemical methods even with the use of high flux reactors.

Radiochemical techniques used in this laboratory for the analysis of Ra^{226} (Rn emanation) give sensitivities higher than those attainable by neutron activation, particularly if the short-lived activation product Ra^{227} is used. Use of high-flux reactors might allow a sensitivity increase by a factor of 10 over present methods. Improved sensitivity through detection of the Ac^{227} daughters could be obtained by irradiations of 4 months to a year. However, these long, intense irradiations would produce uncertainties such as nuclide loss due to severe damage to the samples.

In summary, neutron activation is useful for the analysis of natural U, U^{235}, Th^{232}, Th^{230} and Pa^{231}. It is not advantageous for the analysis of Ra^{226} at the present time, but it may be so in the future. Th^{228} cannot be analyzed by the methods described here and analyses of Ac^{227} and Ra^{228} do not appear feasible.

References

1. G. R. Price, R. Ferretti and S. Schwartz. Anal. Chem. 25 322 (1953).
2. Claude W. Sill and Conrad P. Willis. Fluorimetric Determination of Submicrogram Quantities of Thorium. Proc. Seventh Annual Meeting on Bioassay and Analytical Chemistry at Argonne National Laboratory on October 12-23, 1961. To be published as an ANL report.
3. Theodore Hall. Science 134 449 (1961).
4. J. D. Knight, R. K. Smith and B. Warren. Phys. Rev. 112 259 (1958).
5. J. L. Perkin, L. P. O'Connor and R. F. Coleman. United Kingdom Atomic Energy Authority Report AWRE-0-59/57 (Dec. 1957).
6. L. P. O'Connor and J. L. Perkin. J. Inorg. Nuclear Chem. 13 5 (1960).
7. A. A. Berezin, G. A. Stol'arov, Yu. V. Nikol'ski and I. E. Chelnokov. Atomnaya Energ. 5 659 (1958).
8. R. F. Coleman, B. E. Hawker, L. P. O'Connor and J. L. Perkin. Proc. Phys. Soc. (London) 73 215 (1959).
9. R. C. Koch. Activation Analysis Handbook. New York: Academic Press, 1960.
10. Yu. A. Zysin, A. A. Kovrizhnykh, A. A. Lbon and L. I. Selchenkov. Atomnaya Energ. 8 360 (1960).
11. R. A. Nobles and R. B. Leachman. Nuclear Phys. 5 211 (1958).
12. Richard M. Lessler. Thesis, Univ. California, Berkeley (Oct. 1958); cf. Nuclear Science Abstracts 13: 5818.
13. R. C. Jensen and A. W. Fairhall. Phys. Rev. 109 942 (1958).
14. D. Strominger, J. M. Hollander and G. T. Seaborg. Revs. Mod. Phys. 30 585-904 (1958).

STUDIES ON Ra^{226}, Po^{210} AND Th^{228} IN BOVINE BONES AND TEETH*

Elvira R. Di Ferrante**

Abstract

Bovine jaw bones with teeth were analyzed for Ra^{226} and Po^{210}. An average ratio close to unity for the concentration of the two radioelements in bone and teeth formed after weaning age suggests that estimates of body burden could be based on tooth analyses. Differences were noticed among the Ra^{226} contents of bone ash of different animals such as pigs, cows and deer. The radium concentration in the ash of a pregnant cow was found to be three times that of its fetus, whereas a ratio of thirty was obtained for a porcine sample. In bovine bones the range of values found in the Th^{228} concentration was much smaller than that of Ra^{226} and Po^{210}.

*Manuscript to be submitted for publication.

**Resident Research Associate.

EFFECTS OF RADIATION ON ROTIFERS IRRADIATED AT DIFFERENT AGES

Patricia McClement Failla

Rotifers are microscopic, aquatic metazoans that have been used previously in longevity studies.[1-3] They possess a number of characteristics suitable to an investigation of the effects of exposure to ionizing radiation. These characteristics are described below with particular reference to the type of rotifer studied.

Rotifers are relatively complex animals comprised of at least several hundred cells. The rotifer studied, genus Philodina, has a life-span at room temperature extending to about 30 days, comprised of a period of immaturity lasting about 3 days, a period of sexual maturity lasting about 10 days, and finally a period of declining vigor and senility. These rotifers are all females and reproduce by laying eggs that develop parthenogenetically. On the average, about 5 eggs per day are laid which hatch in about 24 hours at room temperature. It is possible, therefore, to build up a clone of rotifers from a single animal. The members of the resultant genetically homogeneous group can be cultured individually and the production and hatchability of eggs and survival time of each animal scored.

It has been demonstrated that whole-body exposure to radiation of insects and mammals shortens the life span. This effect has been described as an acceleration of the aging process. It is not clear, however, how this reduction of longevity is related to the rate of cell division in different tissues and to damage of a genetic nature. In this connection, the rotifer is useful since no cell division occurs after hatching. There is no possibility, therefore, of repair to a tissue through selective repopulation by the least injured cells. Radiation damage that is transmitted through the germ cells which shows up in subsequent (unirradiated) generations is, however, subject to selective forces in the sense that subsequent generations can only be started from hatched, viable offspring. The parthenogenetic nature of the reproductive process, on the other hand, assures that this genetic damage is not "diluted" by introduction of unirradiated genetic material.

An investigation of some effects of ionizing radiation on rotifers was carried out and has been described previously in detail.[4,5] The irradiated animals were followed for survival time and egg production and hatchability as were a number of generations derived from them. Very little effect was seen in the irradiated animals themselves after a dose of 50,000 r given at one day of age. The hatchability of eggs to form the next

generation was, however, reduced to about 50% of control values, as was the egg production of this first postirradiation generation. The lifespan of subsequent generations was affected much less than the other parameters. By the 13th postirradiation generation, the egg production and egg hatchability were still only about 80% of control values, whereas the survival time was back to normal by about the third generation after irradiation.

Since there is no cell division in the rotifer after it hatches, it is perhaps not too surprising that the irradiated animal, by itself, is very resistant to radiation; however, each of the eggs of these rotifers, presumably single cells at the time of exposure, had to undergo many divisions before hatching as a rotifer consisting of hundreds of cells. It seemed of interest, therefore, that rotifers exposed to 50,000 r at one day of age laid almost the same number of eggs as their unirradiated sisters, and that the hatchability of these eggs was not reduced by more than 50%; for in contrast, while the adult Drosophila (in which there is also essentially no cell division) can withstand tens of thousands of roentgens, 50% of its eggs fail to hatch after doses as low as 200 r. Accordingly, it was decided to study further the egg production and hatchability of irradiated rotifers and subsequent unirradiated generations as a function of dose and time of exposure. Most of the experimental techniques used have been described previously.(4)

Results

Dose-effect curves for the production and hatchability of eggs laid by 7-day-old rotifers are shown in Figure 17. Fifteen rotifers were irradiated at one day of age at each dose level. Since the control rotifers laid an average of about 7 eggs each on the 7th day after birth, each point represents data on at least 60 eggs.

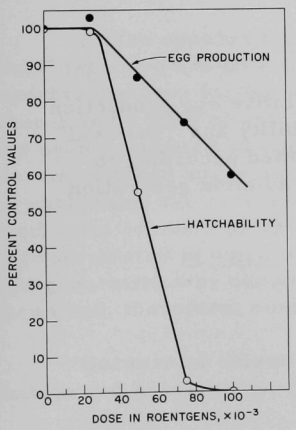

Figure 17

Dose effect on production and hatchability of eggs laid by 7-day-old rotifers

It may be seen that more than 25,000 roentgens must be given to 1-day-old rotifers before either the number of eggs subsequently laid or the hatchability of the eggs is affected significantly.

It was thought that perhaps the unusual radioresistance of the rotifer egg might be a consequence of "recovery" occurring during the 6-day interval between the time of irradiation and the time the egg was laid. Recovery had been looked for in previous experiments[4] by comparing the hatchability of the eggs laid by irradiated rotifers at different ages and, therefore, different times after irradiation. No differences were found. However, since the rotifers had been irradiated at one day of age, and did not lay eggs in appreciable numbers until 4 days of age, it was conceivable that some recovery had taken place which was complete by the time any eggs were laid. Accordingly, a series of experiments was carried out in which rotifers were irradiated with 50,000 r at 1 and at 6 days of age and the numbers and hatchabilities of the eggs laid at 7 days of age compared. The egg production and egg hatchability of the members of the next generation were followed as well. Also, the eggs laid by 7-day-old rotifers were themselves irradiated. The hatchability of these eggs was determined, as was the egg production and hatchability of the first and second generations derived from them.

The results of the above investigation are shown in Figure 18. The relative egg production and hatchability values for the various irradiation conditions are plotted according to postirradiation generation in the following way.

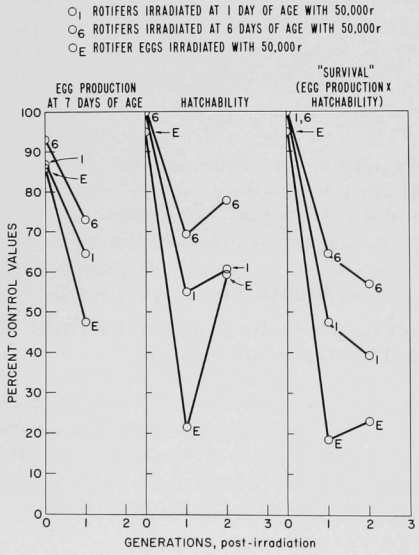

Figure 18

The relative egg production hatchability and "survival" are plotted according to postirradiation generation

The number of eggs laid (in one day) by 7-day-old rotifers irradiated when one day old, six days old, or as eggs (in ovo), represents an effect on the irradiated generation, i.e., 0 postirradiation generation as plotted in Figure 18. The hatchability values for the above eggs, on the other hand, are considered representative of an effect on the first postirradiation generation. The hatchability of the eggs which were themselves irradiated (a surprisingly high 95%) is considered to be an effect on the irradiated generation. To convey an idea of the total effect of diminished egg production and reduced hatchability, the relative "survival" of rotifers to populate the first two postirradiation generations is also shown. These "survival" values are simply the products of the number of eggs laid (relative to control values) to form the generations and the appropriate hatchability figures.

Discussion

Instead of "recovery," the data in Figure 18 show, on the contrary, an increase in radiation effect with an increase in time between irradiation and observation. No such phenomenon was noticed when the animals were irradiated at the same age and the hatchabilities of eggs laid at different ages compared. The most plausible explanation, therefore, is not that the radiation effect requires time to develop but that the more immature egg cells are more radiosensitive. The eggs that were themselves irradiated had been laid at various times during the preceding 24 hours and were, therefore, in different, unknown stages of development at the time of exposure. These eggs, however, were certainly more fully developed than those still in the ovary of the 6-day- or 1-day-old rotifer. The hatchabilities of these groups of irradiated eggs (95, 69, and 55% respectively) are in the order of relative degree of immaturity when irradiated. The very low hatchability (21%) of those eggs laid by rotifers which were themselves eggs when irradiated is consistent with this interpretation.

It also appears that there is only a small effect on egg production if the egg cells are already formed at the time of exposure. This was presumably the case for those eggs laid on the 7th day by rotifers irradiated when 1 and 6 days of age. The fact that the egg production of rotifers which had been irradiated as eggs is so similar to that of rotifers irradiated when already hatched suggests that, on the average, the egg cells were already formed inside the embryos at the time of irradiation. The effect on egg production is much more pronounced in the generation derived from the eggs irradiated in utero or "in utero in ovo." Since the hatchability of this generation was depressed, however, some selection has been introduced and, therefore, some of the effect on egg production may be masked.

Because of selective forces, resulting from both reduced egg production and hatchability, the maximum effects of radiation exposure are

seen in the first and second generations postirradiation. Thereafter, as discussed previously,[4] the values slowly rise toward control levels. However, a levelling-off occurs and some effect is evident after even about 13 postirradiation generations. Since no outside, unirradiated genetic material is being introduced during this time, this depressed equilibrium level (about 80% of control values for both egg production and hatchability) may represent residual genetic damage which cannot be eliminated by selection.

Although quantitative variations in radiation effect have been observed when rotifers are irradiated at different stages of development, no stage has yet been found at which the rotifer even approaches many bacteria in radiosensitivity. The resistance of rotifer eggs is difficult to reconcile with observations on most other rapidly dividing cell systems. Perhaps the necessary genetic material is present in multiple amounts in rotifers so that there is a redundancy of "information." This multiplicity would serve to alleviate the consequences of chromosome breaks or other genetic damage and thereby confer a high degree of radioresistance. Paucity of information concerning the genetic system of the rotifer, however, leaves this suggestion still in the realm of speculation at the present time.

Summary

Dose-effect curves are given for the number and hatchability of eggs laid on the 7th day by rotifers irradiated at one day of age. These are very radioresistant parameters, yet, as shown in a previous study, they are more sensitive indicators of radiation damage than survival time. In an effort to elucidate reasons for the radioresistance of rotifers, they were exposed to 50,000 r at different ages, i.e., as eggs, at 1 day of age, and at 6 days of age. The number of eggs laid on the 7th day by the exposed generation and by members of the next (unirradiated) generation was determined as was the hatchability of these eggs. The greatest effect is apparent in the hatchability of eggs to form the first postirradiation generation and the egg production of this generation. The variation of these parameters with the age of the rotifer at the time of irradiation indicates that the most immature egg cells are the most radiosensitive. Nevertheless, 50,000 r delivered at the most sensitive stage only reduced subsequent egg production to about 50% and hatchability to 20%.

The technical assistance of Janet M. Prince is gratefully acknowledged.

References

1. H. S. Jennings and A. S. Lynch. Age, Mortality, Fertility and Individual Diversities in the Rotifer Proales sordida gosse. I. Effect of Age of the Parent on Characteristics of the Offspring. J. Exptl. Zool. 50 345 (1928).

2. Albert I. Lansing. Some Effects of Hydrogen Ion Concentration, Total Salt Concentration, Calcium and Citrate on Longevity and Fecundity of the Rotifer. J. Exptl. Zool. 91 195 (1942).

3. Albert I. Lansing. A Transmissible, Cumulative Reversible Factor in Aging. J. Gerontology 2 228 (1947).

4. Patricia McClement. Some Effects of Radiation on Rotifers and their Unirradiated Progeny. Annual Report on Research Project. Columbia University, NYO-2784 (July 1, 1959). p. 151.

5. Patricia McClement Failla. Some Effects of Radiation on Rotifers and their Unirradiated Progeny. Radiation Research 11 442 (1959) (Abstract)

THE EFFECT OF METEOROLOGICAL VARIABLES UPON RADON CONCENTRATION THREE FEET ABOVE THE GROUND

Harry Moses, Henry F. Lucas, Jr., and
Gunther A. Zerbe

I. Introduction

There have been numerous investigations concerning the concentration of radon in the lower layers of the atmosphere, examples of which are reported by Wright and Smith,[1] Miranda,[2] Gale and Peaple,[3] and Wilkening.[4] Although the averaging periods were often neither comparable nor the most desirable - ranging from several minutes to many hours - the essential features of the diurnal and seasonal variations were determined. In nearly all of the studies, attempts were made to relate the effect of meteorological variables on radon concentration, but the conclusions left much to be desired. For example, Wilkening[4] did not discuss the effects of precipitation, while Gale and Peaple[3] and Wright and Smith[1] considered this factor significant. The role of atmospheric pressure has eluded convincing argument one way or the other. Even the effect of wind speed was discounted by Gale and Peaple.[3]

The Radiological Physics Division of the Argonne National Laboratory made consecutive eight-hour measurements of radon concentrations at three feet above the ground, beginning at 0845 each Monday and ending at 1645 the following Friday from August 20, 1956 through September 30, 1957. These measurements were conducted about one mile from the Meteorology Laboratory where values of a rather extensive set of meteorological variables are continuously recorded.[5] Thus, a body of data became available to shed light on some of the controversial aspects of this problem and to gain further insight into the meteorological processes affecting the distribution of radon. The techniques for obtaining the radon and meteorological measurements are described elsewhere.[5,6]

The study presented in this paper consists of two sections: 1. case studies based on a time-series comparison of radon and pertinent meteorological variables for periods of clear weather, extremely windy weather, unusually moist ground, and snow cover, and 2. a climatological summary of the radon measurements as shown by relative frequency diagrams for the four seasons, time of day, and various ground conditions.

II. Case Studies

It is commonly agreed that radon concentrations observed at a point above the ground are affected by the rates of: 1. radioactive decay,

2. transport by the wind (advection), 3. emanation from the soil, and 4. atmospheric diffusion. With a radioactive half-life of 3.825 days, the effect of decay in eight-hour radon samples is negligible, i.e., about 5%.

The advection of radon by the wind from an area of higher or lower concentrations is a factor which cannot be discounted, as shown previously by Moses, Stehney and Lucas,(7) but only an inconclusive indication of this effect is shown in Figure 19. All of the case studies, Figures 19-22, demonstrate clearly the effects of the remaining two processes, i.e., emanation from the soil and atmospheric diffusion.

A. Clear Weather Conditions with Dry Ground

The readings shown in Figure 19 are typical of conditions where intense thermal convection occurs during the daytime and a strong nocturnal inversion develops at night. During this weather regime, the diurnal amplitude of radon concentration is high with highest values occurring just before sunrise. As may be seen from this figure, extremely high radon concentrations were observed in the early mornings of the 11th, 12th, and 13th, with a maximum of 1.310 pc/liter on the 12th. Although concentrations appear high during the day following a high nighttime value, those readings may be misleading because of averaging periods used. As shown in a previous paper,(7) during midday the radon concentrations may become quite low, even though high concentrations are observed in the early morning.

Since the ground was dry during September 11-14, 1956, one may ascribe the variations in radon concentrations to variations in the diffusive capacity of the atmosphere. The 0.24 inch of rain which fell during the evening of the 9th probably reduced the emanation rate and contributed to the relatively lower daytime readings on the 10th.

It is of interest to note that during the afternoon of the 13th, a cold front passed the station as evidenced by the following: the veering of the wind direction from south to northwest and later to north, the increase in wind speed, the rise in pressure, and the cooling and drying of the air. Observe that the maximum temperature on the 14th was 21.4°C compared with 33.3°C on the previous day. The maximum radon concentration during the early morning of the 14th was 0.555 pc/liter, appreciably lower than 0.957 pc/liter observed during the previous morning. Since the stability was lower during the early morning of the 14th than on the 13th, one cannot convincingly ascribe the reduction in radon concentration to mass transport; the change in the diffusion rate may well account for the difference.

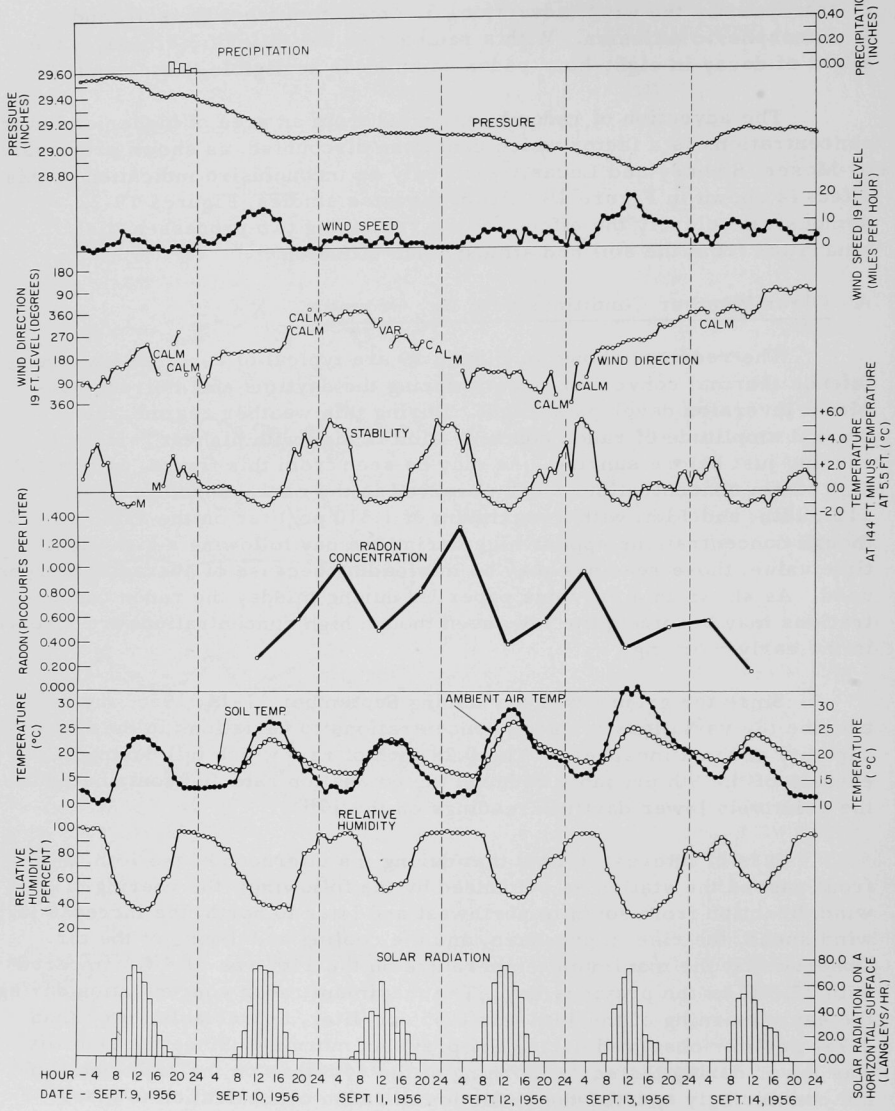

Figure 19

Case study of radon concentrations with intense thermal convection during day and strong nocturnal inversion during night

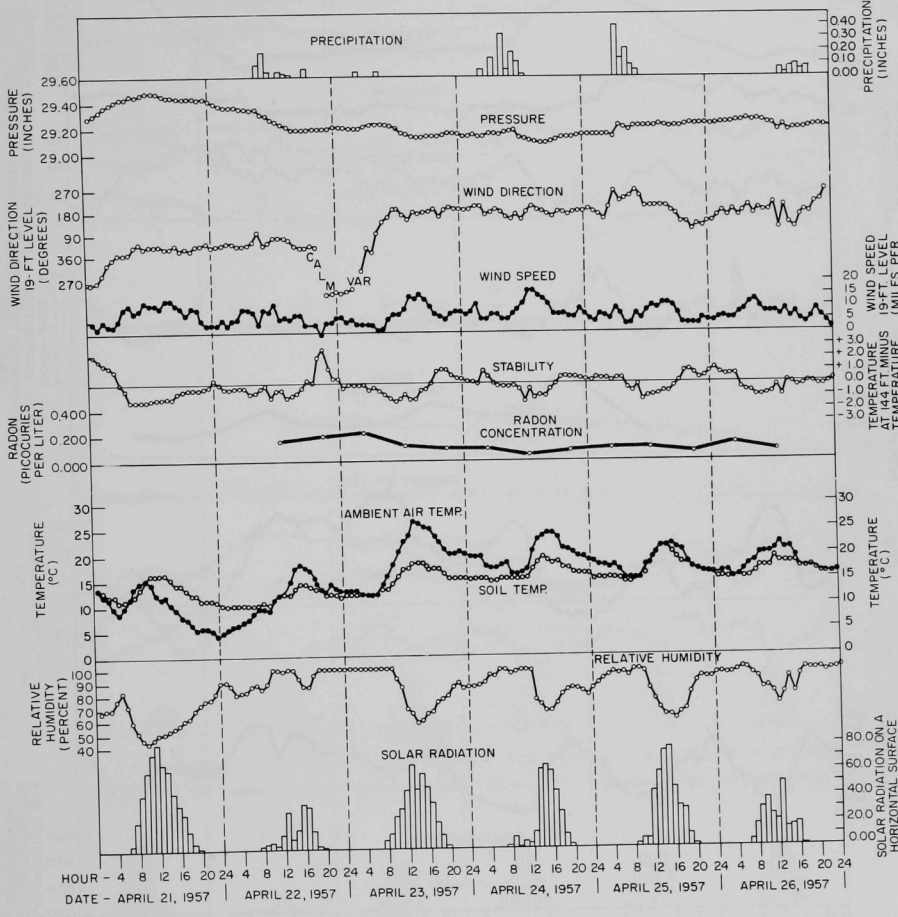

Figure 20

Case study of radon concentrations with extremely wet ground conditions

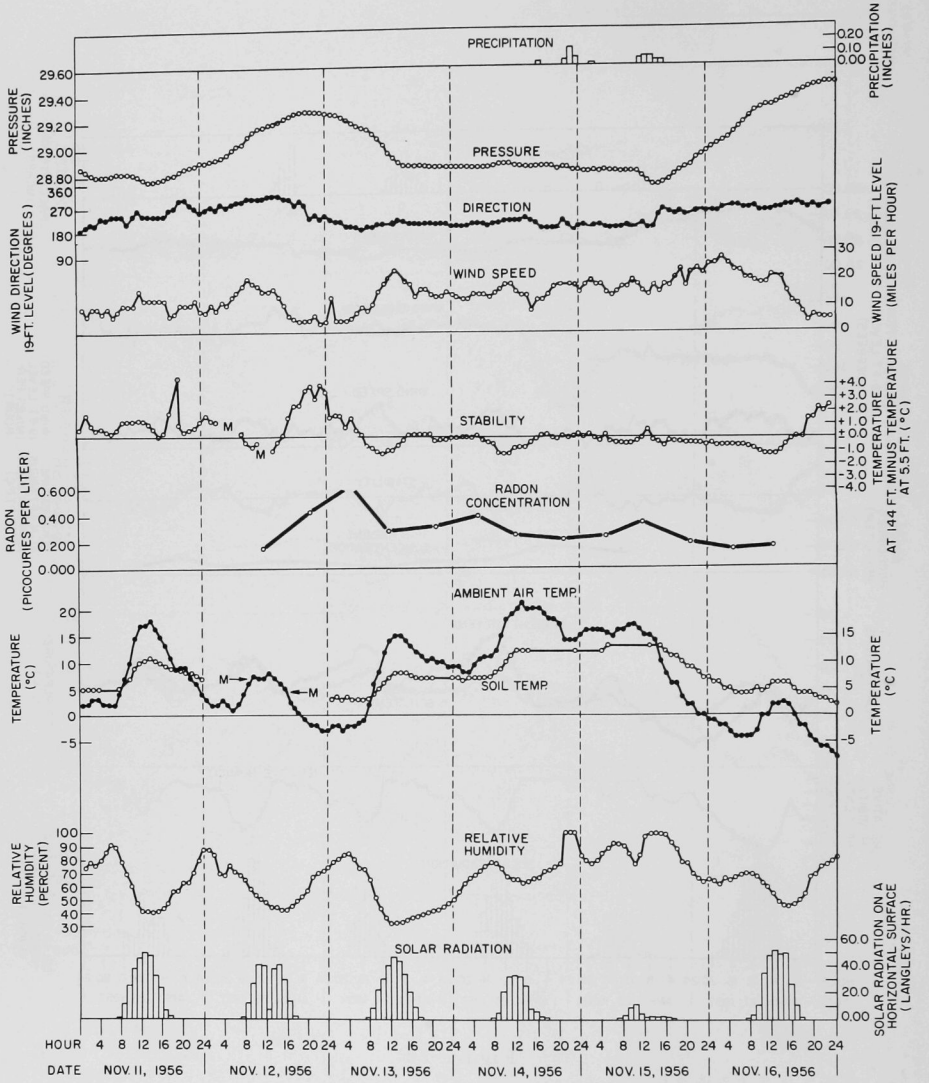

Figure 21

Case study of radon concentrations during strong winds

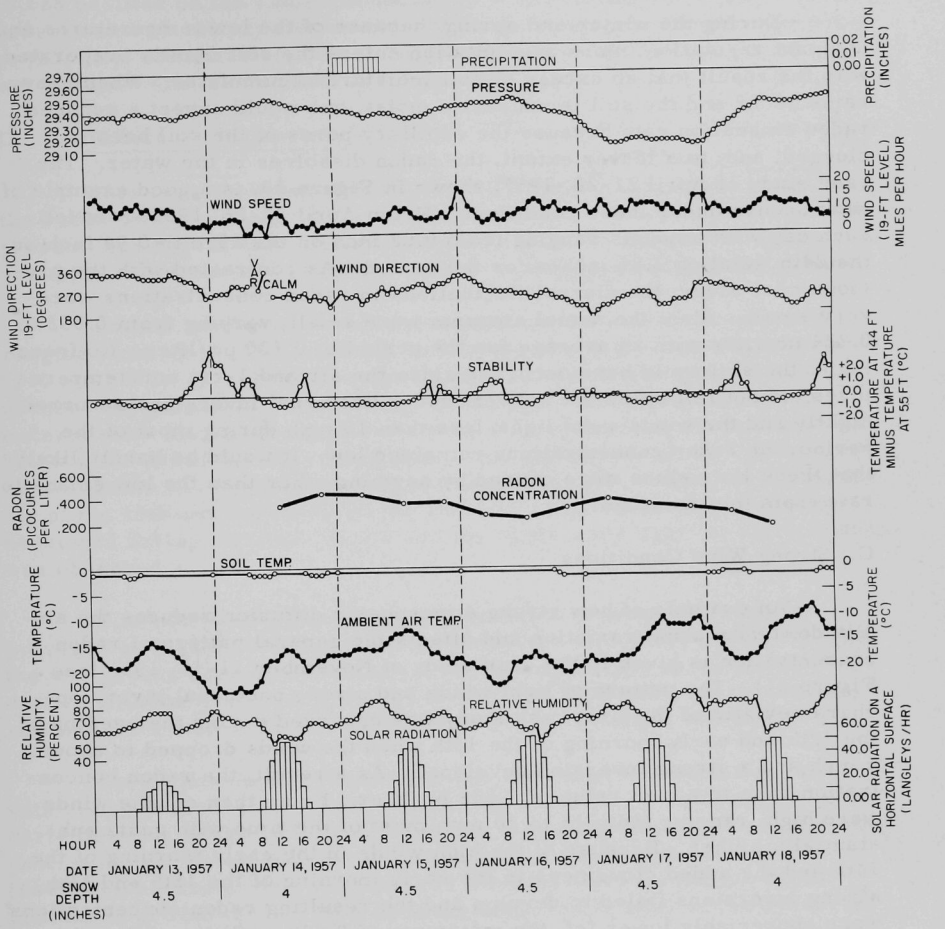

Figure 22

Case study of radon concentrations when a snow cover is present

B. Wet-Ground Conditions

During the winter and spring, because of the low temperatures and dormant vegetation, more precipitation enters the soil than is evaporated, with the result that an excess of soil moisture accumulates. When heavy rains occur and the soil is unusually moist, one would expect a reduced radon emanation rate because the capillary pores of the soil become clogged, and, to a lesser extent, the radon dissolves in the water. The case study of April 21-26, 1957, shown in Figure 20, is a good example of what occurs under these conditions. From April 22-26, 1956, rain fell each day with amounts ranging from 0.08 inch on the 23rd to 0.94 inch on the 24th, totaling 2.81 inches for the period. As contrasted with the previous case study, the diurnal fluctuations in radon concentrations were very small. Also, the actual amounts were small, varying from 0.052 to 0.224 pc/liter with an average for the period of 0.120 pc/liter. No freezing of the soil could have occurred since the air and 1-cm soil temperatures did not fall below 5°C. Even though nocturnal inversions occurred nightly and the winds were light, less than 10 mph during most of the period, the radon concentrations remained low. It would be hardly likely that these low values were caused by anything other than the low emanation rate from the moist soil.

C. Strong Wind Conditions

An example of how strong atmospheric diffusion reduces the amplitude of the diurnal variation and affects the general pattern of radon concentration is given in the case study of November 11-16, 1956 (see Figure 21). The pattern of light winds and strong nocturnal inversion characteristic of the first case study was observed during the evening of the 12th and early morning of the 13th when the winds dropped to about 5 mph and a strong inversion developed. As a result, the radon concentration rose to a high value of 0.628 pc/liter. From then on, the winds were high, ranging from 15 to 20 mph most of the time with gusts substantially higher. Because of the high winds in the early morning of the 14th and the added cloudiness in the early morning of the 15th and 16th, strong inversions failed to develop and the resulting radon concentrations were appreciably lower (cf. the maximum of 0.628 pc/liter on the 13th with 0.399 pc/liter on the 14th).

The wet ground caused by the 0.50 inch of rain which fell during the 14th and 15th in combination with the high winds further reduced the radon concentrations on the 15th and 16th. The lowest early morning reading of the series occurred the next day, November 16th, when a reading of 0.154 pc/liter was recorded. At this time, the wind was highest for the period, reaching 30 mph.

It may be of interest to note that the highest early morning value (0.628 pc/liter on the 13th) was recorded with a falling barometer and the lowest value (0.154 pc/liter on the 16th) with a rising barometer. In all probability, the diffusion rate as determined by wind and stability and the wet ground were the dominating influences.

D. The Effect of a Snow Cover

This case study based on data for January 13-18, 1957 shows how the radon concentrations varied when a snow cover of 4 to $4\frac{1}{2}$ inches was present (see Figure 22). The striking feature is the absence of the diurnal variation characteristic of clear weather with light winds and dry ground.

The air temperature throughout this period was extremely cold ranging from -8 to -25°C, and the soil temperature at 1 cm varied from -0.8 to -1.5°C. It is difficult to tell whether the soil was actually frozen at these temperatures. Tests made in the past indicate that the ground under a snow blanket remains soft, even at temperatures several degrees below 0°C. All of the days were sunny, and all but two of the nights were clear; clouds were present during the evening of the 14th and early morning of the 15th and similarly on the 16th and 17th. Although inversions developed during the clear nights and the winds were light, no radon buildup was observed.

It is somewhat surprising that the radon concentration values averaged as high as 0.320 pc/liter as compared with 0.120 pc/liter during the wet-ground case study. Likely contributing factors are reduced convection with the presence of a snow cover, and difference in the amount of soil moisture or a different distribution of soil moisture with depth.

These data appear to indicate that the radon concentration falls with rising pressure and rises with falling pressure. For example, in the early morning of the 18th, with a sharply rising barometer, the radon concentration was lower than during the previous eight-hour observation (1645-0045). Ordinarily, readings for the 0045-0845 period are higher than those of 1645-0045. This anomaly occurred in spite of the presence of light winds and a nocturnal inversion. Other instances of an apparent pressure effect may be seen in Figure 22. Nevertheless, more data than are presented in a single case study are needed to draw valid conclusions.

III. Seasonal Distribution of Radon Concentration

A. Treatment of the Data

In this portion of the study, the data were divided according to whether the ground was wet or dry as determined by the amount of precipitation which fell within the previous 24-hour period. If less than

0.04 inch of precipitation fell within 24 hours preceding the end of the current eight-hour period, the ground was considered dry. If 0.10 inch or more fell within this period, the ground was considered wet. The measurements were omitted when the precipitation ranged from 0.04 to 0.09 inch. It should be pointed out, however, that these definitions are arbitrary and that the ground may actually remain wet for periods substantially exceeding 24 hours. This is especially common in spring.

The data were further subdivided according to season. Instead of the astronomical divisions, winter was assumed to consist of December, January, and February; spring - March, April, and May; summer - June, July, and August; and fall - September, October, and November. Since the measurements were made for the period August 20, 1956 to September 30, 1957, the summer measurements included August data for 1956 and 1957, and similarly, the fall data contained September measurements for the two years.

It is also to be noted that the radon concentration measurements which began at 0845 on Monday and ended on 1645 on Friday were taken on Central Standard Time from October 29, 1956 through April 29, 1957 and on Central Daylight Time during the remainder of the measuring period.

The percentage frequency diagrams (Figure 23) show the distributions of radon concentrations under wet and dry ground conditions for each season and for each eight-hour period. Presenting the frequencies as percentages of the total in each category allows the ready comparison of the numerous data obtained under dry-ground conditions with the substantially fewer measurements obtained under wet-ground conditions. Values of the mean and standard deviation and the number of cases are presented in Table 8.

B. The Early Morning Curves (0045-0845)

The most pronounced seasonal differences occur in the measurements for this period. In the summer and fall, with the frequent occurrence of light winds and strong inversions, large accumulations of radon are observed. As a result, these curves are skewed to the right. The criterion adopted for wet- and dry-ground conditions appears to separate the two curves significantly. In the spring, the ground is quite moist during a major portion of the time because of snow melt and the low evaporation rate. For this reason, the wet and dry curves are not significantly different, and the distribution patterns exhibiting low radon concentration values are what one would expect under wet-ground conditions. In winter, the number of observations with rainfall 0.10 inch or greater were too few to allow a valid comparison of the two curves.

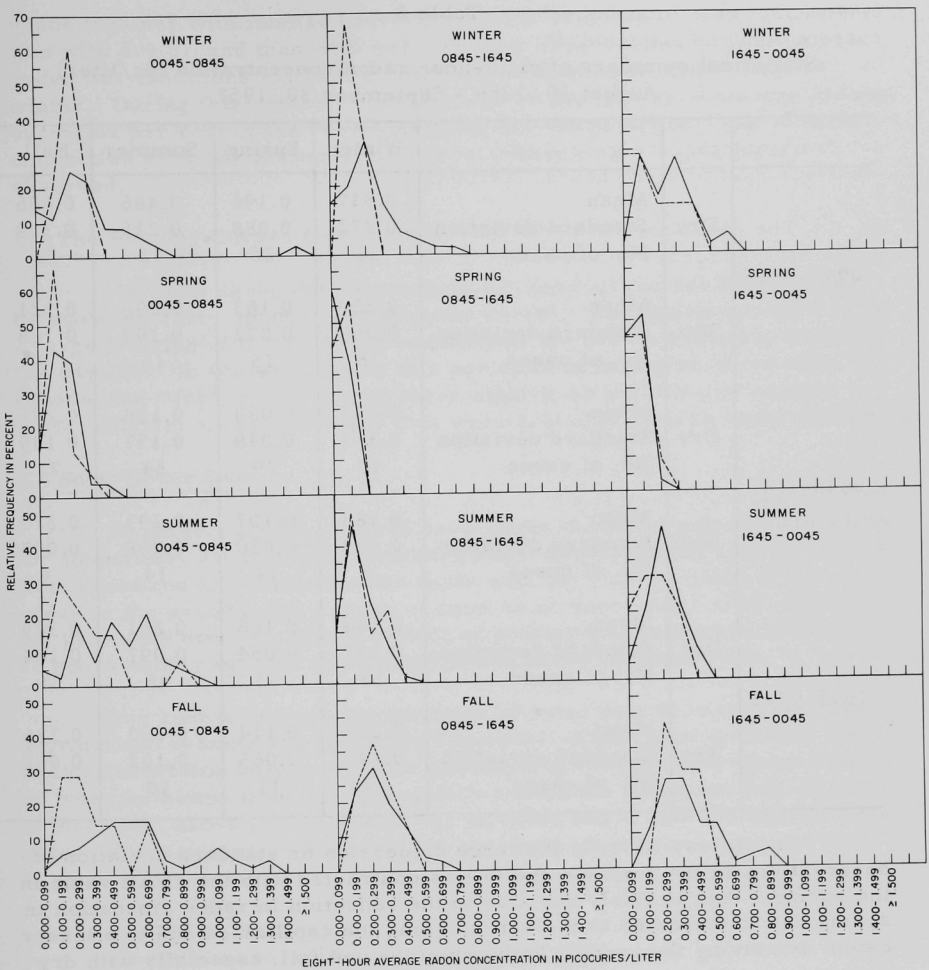

Figure 23

Relative frequency distribution of eight-hour radon concentrations.

——— represents dry ground conditions, i.e., less than 0.04 in. of precipitation in 24-hour period ending with 8-hour period under consideration

– – – – represents wet ground conditions, i.e., 0.10 inch or more precipitation in 24-hour period ending with 8-hour period under consideration.

Table 8

Statistical summary of eight-hour radon concentration (pc/liter)
August 20, 1956 - September 30, 1957

			Winter	Spring	Summer	Fall
0045-0845	Dry	Mean	0.347	0.196	0.486	0.606
		Standard deviation	0.272	0.088	0.215	0.319
		No. of cases	36	28	42	52
	Wet	Mean	0.250	0.163	0.296	0.321
		Standard deviation	0.063	0.072	0.199	0.168
		No. of cases	5	15	13	7
0845-1645	Dry	Mean	0.261	0.089	0.198	0.281
		Standard deviation	0.164	0.048	0.157	0.139
		No. of cases	46	39	54	72
	Wet	Mean	0.183	0.107	0.193	0.275
		Standard deviation	0.048	0.050	0.098	0.097
		No. of cases	6	14	14	8
1645-0045	Dry	Mean	0.304	0.108	0.261	0.389
		Standard deviation	0.147	0.054	0.097	0.184
		No. of cases	35	33	45	54
	Wet	Mean	0.207	0.114	0.200	0.336
		Standard deviation	0.140	0.063	0.102	0.082
		No. of cases	7	11	10	7

Of interest, also, is the large dispersion or standard deviation of observations in the summer and fall as contrasted with the small value in the spring. This is likely due also to the reduction in radon emanation in spring due to the water in the soil clogging the capillaries and to a lesser extent dissolving the radon. In the summer and fall, especially with dry ground, the diffusive capacity of the atmosphere is the controlling factor in determining the observed radon concentrations.

C. The Daytime Curves (0845-1645)

An outstanding feature of the daytime curves is the similarity between the wet and dry curves especially in summer and fall. When the ground is dry and the skies are clear, strong convection tends to diffuse the radon over deep layers, so that the concentrations observed at the ground are comparable to those which occur when the ground is wet - a condition associated with reduced convection. In the spring, the higher

winds together with intense convection yields even lower radon concentration with dry ground than with wet. Too few observations were available under wet conditions to allow a valid comparison of the two curves in winter. During this period, a snow cover of one inch or more was present during 61 per cent of the observations in the dry category. The reduced convection probably accounts for the relatively higher radon values observed.

D. The Evening Curves (1645-0045)

The evening curves in summer, fall, and spring are intermediate between the early morning and daytime curves. During the summer, when a large fraction of the period is in daylight, the curves resemble those of the daytime. In winter, most of this period is in darkness, but in this season, the "dry" curves for all three eight-hour periods are similar. An insufficient amount of "wet" data were available to draw valid conclusions.

E. Snow Cover Data

To determine the effect of snow cover the radon concentration data for December, January, and February were divided into two parts: the first contained all measurements made with one inch or more of snow present; the second with a trace of snow or no snow cover at all and with the provision that less than 0.04 inch of precipitation occurred within the 24 hours ending with the eight-hour period under consideration.

Per cent frequency distributions of these data for early morning, daytime and evening are plotted in Figure 24. This figure indicates the rather surprising result, viz., the presence of a snow cover of one inch or more in winter does not appreciably reduce the radon concentrations at three feet above ground (Table 9). In other words, the amounts of radon observed are comparable with those observed when only a trace or less of snow is present.

IV. Summary of Results

Although the amount of data included in the case studies is not enough to establish quantitative relationships between radon concentrations and meteorological variables, useful qualitative information may be derived. The frequency diagrams are based on a greater number of observations though still not enough to yield irrevocable conclusions. Nevertheless, the results obtained in this study, when examined in the light of the work performed by other investigators,[1,3,4] appear to be valid.

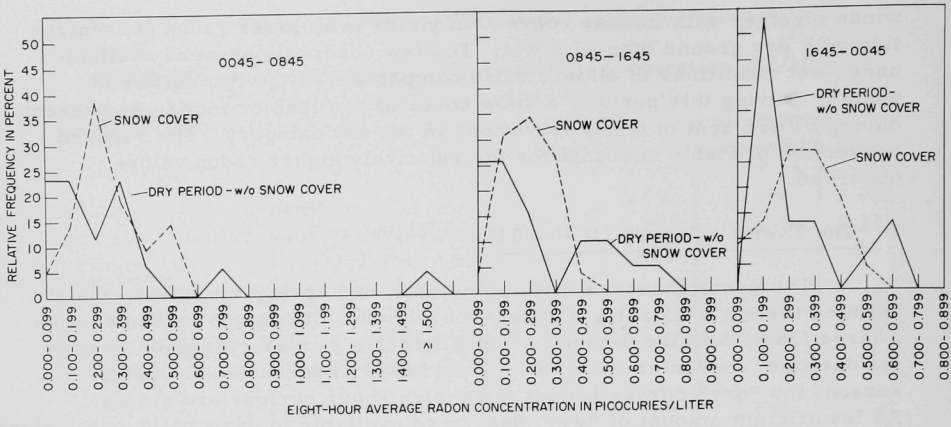

Figure 24

Relative frequency distributions for December 1956, January and February 1957, comparing 8-hour radon concentrations measured over ground with a snow cover of one inch or greater and with no snow cover and dry ground conditions. No snow cover is defined as a trace or less, and dry ground as the ground condition where less than 0.04 in. of precipitation occurred during the 24-hour period ending with the 8-hour period under consideration.

Table 9

Effect of snow cover on eight-hour radon concentrations (pc/liter)
December 1, 1956 - February 28, 1957

		Snow cover present - one inch or more	Dry conditions - trace or less of snow present
0045-0845	Mean	0.307	0.318
	Standard deviation	0.137	0.344
	No. of cases	21	17
0845-1645	Mean	0.246	0.271
	Standard deviation	0.094	0.219
	No. of cases	26	19
1645-0045	Mean	0.295	0.283
	Standard deviation	0.132	0.182
	No. of cases	22	15

The above investigation illustrates the following:

1. With dry ground, when strong convection occurs during the daytime and a pronounced inversion develops at night, the range or radon concentration is large; i.e., high concentrations are observed at night and low concentrations during the day.

2. With wet ground, the amount of radon measured is appreciably reduced. This is shown by: a. the low values observed in the case study of April 21-27, 1957, b. the low spring time values, and c. the significant difference in the average concentrations of radon observed during the early morning "wet" and "dry" frequency diagrams for summer and fall. The above case study for a period of excessive rainfall and associated wet ground also illustrates the marked reduction in amplitude of the diurnal variation of radon concentration.

3. During high winds diffusion rates are high and therefore lower radon concentrations are observed near the ground, as is indicated by the case study of November 11-16, 1956.

4. The daytime frequency diagrams for wet and dry conditions during summer and fall indicate similar distributions. It appears that the similarity is brought about by an interesting combination of factors. With dry ground, large amounts of radon are released, but the vigorous convection prevailing during dry periods diffuses the radon so that relatively small amounts are observed in the lower layers. With wet ground, a substantially lesser amount is released, but the reduced convection due both to the cloudiness associated with rainy periods and the utilization of solar radiation in evaporating water from the wet ground surface retards diffusion. As a result, the expected difference between radon concentrations during wet and dry conditions is minimized.

5. It is well known that a snow cover is an efficient thermal blanket preventing heat loss from the soil to the air above. The results of this study indicate that a snow cover of four inches or less is an inefficient barrier for the emanation of radon. In the case study of January 13-18, 1957, where at least four inches of snow was present throughout, relatively high values of radon were observed. Further (Figure 24), the frequency distributions for radon during the presence of a snow cover of one inch or more and during nearly bare ground (a trace or less of snow) under dry conditions, show that the observed concentrations are comparable. Thus, a snow cover of the order of four inches or less probably offers little obstruction to the release of radon from the soil.

6. In the above case study for conditions under snow cover, the changes in radon concentration and pressure rise or fall appeared to be related. Of course, with so few examples, it would be folly to conclude

that a relation exists. However, it might be worth while to look for an amplified pressure effect during the presence of a snow cover because of the greater porosity of snow as compared with that of soil.

The authors thank Mr. Frank C. Kulhanek and Mrs. Martha S. Sundquist for their help in reducing the data and Mr. Frank H. Ilcewicz for aid in making the radon measurements.

V. References

1. J. R. Wright and O. F. Smith. The variation with meteorological conditions of the amount of radium emanation in the atmosphere, in the soil gas and in the air exhaled from the surface of the ground at Manila. Phys. Rev. 5 459-482 (1915).

2. H. A. Miranda. The radon content of the atmosphere in the New York area as measured with an improved technique. J. Atmospheric Terrest. Phys. 11 272-283 (1957).

3. H. J. Gale and L. H. J. Peaple. A study of the radon content of ground-level air at Harwell. Intern. J. Air Pollution 1 103-109 (1958).

4. M. H. Wilkening. Daily and annual courses of natural atmospheric radioactivity. J. Geophys. Research 64 521-526 (1959).

5. H. Moses and J. H. Willett. Argonne National Laboratory five-year climatological summary, July 1949-June 1954. Argonne National Laboratory Report ANL-5592 (1955).

6. H. F. Lucas, Jr. Improved low-level alpha scintillation counter for radon. Rev. Sci. Instr. 28 680-683 (1957).

7. H. Moses, A. F. Stehney, and H. F. Lucas, Jr. The effect of meteorological variables upon the vertical and temporal distributions of atmospheric radon. J. Geophys. Research 65 1223-1238 (1960).

CONVECTIVE TURBULENCE WIND TUNNEL PROJECT
CALIBRATION TOWING CHAMBER

Edward J. Kaplin*

Introduction

A calibration towing chamber has been designed and constructed for the purpose of determining accurate calibration curves for velocity sensing devices in a speed range of from 0.10 fps to 1.50 fps.(1) This apparatus development was conducted at New York University to refine the techniques and equipment necessary in the performance of scale model smoke diffusion studies previously reported.(2-5) The work was accomplished, in part, under Argonne subcontract #31-109-38-743.

In the model smoke diffusion experiments previously reported,(3,5) the wind tunnel velocity profiles were based on the assumption that the calibration curves (air speed vs hot-wire current) for the hot-wire anemometer probes followed a power law distribution between 0 and 8.0 fps. The slope of this calibration line represented the "best fit" to points determined by timing smoke puffs over a measured distance in the wind tunnel for a speed range of from about 1.0 to 8.0 fps.

Determination of calibration points for these hot-wire probes in the towing chamber between speeds of about 0.10 to 1.60 fps, along with points determined in the wind tunnel for speeds between 0.60 and 7.50 fps produced a new calibration curve that differed from a power law distribution. The deviation from the power law is particularly evident at speeds less then 1.0 fps.

This new calibration curve for the hot-wire probes will have relatively little effect on the results and conclusions drawn from smoke diffusion studies previously reported. In only a few instances had the velocity profile in the wind tunnel been determined on the basis of air speeds significantly less than 1.0 fps.

The new calibration curve will be used exclusively in all future experiments and will be particularly significant since these tests are expected to involve more low-speed (less than 1.0 fps) measurements.

Apparatus

The calibration towing chamber is shown in Figure 25. The chamber itself was constructed of wood, aluminum and Plexiglas. The inside dimensions of the chamber are 18" wide, 96" long and 24" high. The front of the chamber consists of three Plexiglas window doors for convenient entrance

*Associate Research Scientist, College of Engineering, New York University. This work supported in part under Argonne National Laboratory subcontract 31-109-38-743.

and viewing inside the chamber. The ends of the chamber are aluminum plates. The aluminum was selected for ease of construction and to provide for free transfer of heat in and out of the chamber, assuring that the enclosed air would be thermally homogeneous. (Testing in the chamber later indicated that this thermal homogeneity was not desirable and the end plates were covered with $\frac{1}{2}$" Celotex for insulation.) The probe mount carriage was constructed from ground flat-stock to assure parallel surfaces. The carriage travels on two sets of miniature flanged ball-bearing wheels which position and hold it to a track. The track is a special Starrett Straight Edge No. 380. This assures parallel surfaces and clean sharp edges upon which the flanged bearings may roll to provide smooth traverses for the carriage during towing. The probe mounts and supports have been designed to afford the greatest flexibility in usage. When used for the hot-wire probes, they provide for multipositioning of the probes as desired. The wires from the hot-wire probes are cabled and ride freely along a support rod attached to the chamber end plates. These wires are connected through terminals on the end plates to the anemometer bridge circuit. Although the carriage is driven by an 1800-rpm synchronous motor, its rotation rate is geared down to 450 rpm to drive a selected series of spur gears and a screw drum. Motion of the drum is transmitted to the carriage by a thin braided model-aircraft control cable. Forward or reverse movement of the carriage is determined by the direction of rotation of the synchronous motor. A control panel for the towing system provides for full or semi-automatic operation. At either end of the chamber along side of the track are a pair of reset limit switches which are activated by contact with the carriage bed. One switch at each end is used to shut off the power to the motor and to activate simultaneously a magnetic brake to halt the motor shaft at the completion of a carriage traverse. The other two switches are provided to start and stop an electric timer. These timer switches are set to give the time required for the carriage to travel 66".

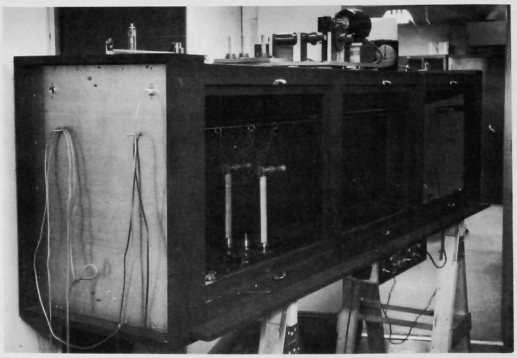

Figure 25

Over-all view of calibration towing chamber

They are positioned to eliminate the effects of carriage acceleration and deceleration. The speed determined by the timer is used as a check on the gear drive system.

Operation Technique

The calibration towing chamber has been designed and constructed to allow the calibration of almost any type of velocity-measuring device capable of being attached to its carriage. As of this time, only velocity probes of the hot-wire type have been calibrated. All discussion of the towing chamber will be based only on those results.

1. Hot-Wire Anemometer System

As used at the $3\frac{1}{2}$-x 7-foot Wind Tunnel, the hot-wire system is a simple bridge circuit. The probe tip is a platinum wire (0.001"). The operational procedure is as follows: with the hot-wire probe capped off from the airstream, a galvanometer is brought to null and locked with a current of 200 ma passing through the bridge circuit. The probe is then uncapped and exposed to the "moving" airstream. The variable bridge resistances are adjusted to return the galvanometer to zero. The resultant change in current is then related to the airstream velocity. The current change is reported as a number ΔI. Depending upon the milliammeter used, 4 ΔI or 5 ΔI is equivalent to the actual current change in milliamperes.

2. Towing Chamber Operational Procedure

In operation, a hot-wire probe is placed (capped) on a mount inside the towing chamber. The cap and probe are allowed to come to temperature of air in the enclosed chamber, and the hot-wire bridge is brought to null at a "zero" of 200 ma. The towing chamber is opened and the probe cap is removed. The chamber is reclosed, and air disturbances are allowed to die out (some disturbance must remain due to the chimney effect of the hot wire but this local effect does not seem to permeate the entire chamber). The carriage and probe are then set in motion at a speed predetermined by the spur gear combinations employed. The hot-wire bridge is rebalanced with the probe in motion, and a ΔI value proportional to change current is determined. The value of ΔI plotted against the known velocity results in a calibration curve for the given hot-wire probe (see Figure 26).

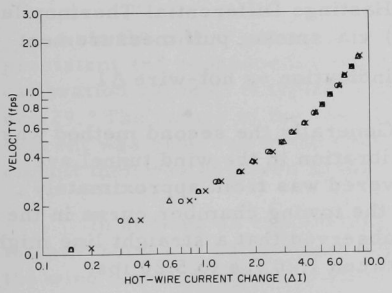

Figure 26

Velocity calibration. Hot-wire probe #3. Towing chamber test points.

The calibration procedure as described is generally trouble free. If for some reason the carriage is derailed in operation or, through improper switching, allowed to progress to either end of the tow chamber while still at a driving speed, the towing cable is the weakest link and it usually breaks at its connection point with the carriage.

Discussion of Results

The calibration curve determined for a given probe is quite stable and reproducible. Most variations can be accounted for by inherent inaccuracies in the readings taken from the milliammeter. The suppressed zero meter is marked off in 40 units from 30 to 70 (I_0 (200 ma) = 38.0). The scale is an arc segment about 3.5 inches long, and readings are estimated to the nearest tenth of a division. With reasonable caution the error in reading is not expected to exceed $\pm$ 0.10 of a division.

A plot of representative calibration points determined in the towing chamber are presented in Figure 26. The velocity values range from a minimum of 0.11 fps to 1.57 fps. It is observed that it is not possible to fit any form of straight line to any significant number of consecutive points.

To extend the calibration curve over the full range of wind speeds normally observed in the wind tunnel, the same hot-wire probe used in the towing chamber was calibrated directly in the wind tunnel. This technique, as previously described, involved setting the wind tunnel at a given speed and noting the corresponding ΔI value for the hot-wire anemometer. The wind tunnel speed was determined by one of two methods:

1. Direct: timing of smoke puffs over a measured distance vs hot-wire ΔI

2. Indirect: a) calibration of a Hastings Differential Thermopile (non-directional) via smoke puff measurement

   b) Hastings meter indication vs hot-wire ΔI

Both techniques gave the same results. Generally the second method was used for convenience. The results of calibration in the wind tunnel are shown in Figure 27. The speed range covered was from approximately 0.60 fps to 7.50 fps. The curve overlaps the towing chamber curve in the range of from 0.60 fps to 1.60 fps. It is observed that a straight line might be fitted to the wind tunnel test points between 1.20 fps to 5.20 fps.

When the results of calibration in the towing chamber and in the wind tunnel are combined, a best estimate single calibration curve can be determined as shown in Figure 28.

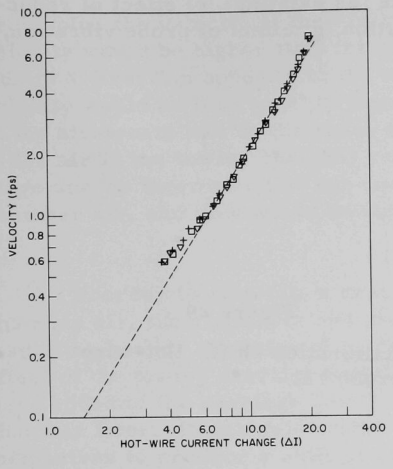

Figure 27

Velocity calibration. Hot-wire probe #3. Wind-tunnel test points.

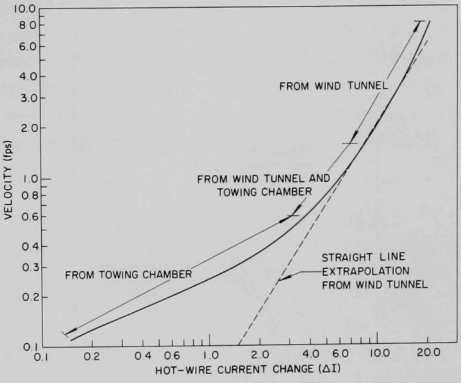

Figure 28

Velocity calibration curve. Hot-wire probe #3.

Calibration Shift Due to Presence of Carriage

When the towing chamber was first put into operation, the chamber was filled with smoke, and observations were made to observe the possible presence of motion in the air enclosed in the chamber. No noticeable motion occurred with the carriage and probe stationary. Only slight disturbances were noticeable in the lee of the moving carriage, and no motion was observable in the vicinity of the probe tip.

In the initial phases of operation in the towing chamber a marked, persistent and reproducible shift was observed between the two derived calibration curves. A typical instance of this translation is noted in Figure 29. The nature of the translation is such that for a given velocity more current was required in the towing chamber to balance the hot-wire bridge circuit than was required in the wind tunnel.

In seeking an explanation for the observed calibration shift, a systematic series of calibrations was performed in the towing chamber and in the wind tunnel designed to eliminate possible sources of the observed discrepancy. Among the possible sources of error that were investigated and eliminated were a) radiational heat losses, b) lead wire resistance, c) wall

effects, d) effect of air stream turbulence (as existing), e) effect of reducing zero levels, f) effect of probe orientation, g) effect of probe vibration, and h) effect of ambient temperature.

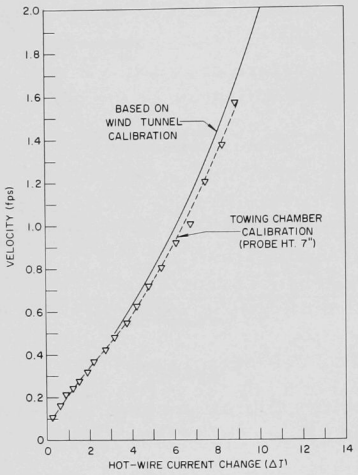

Figure 29

Calibration shift. Hot-wire probe #3.

After all of the previous investigations had been completed without success in regard to determining an apparent cause for the calibration shift, the occasion presented itself to start a calibration run in the towing chamber with the outside room air and the enclosed chamber air initially at a uniform cool temperature. The outside room temperature was, however, increasing due to the addition of heat. Some heat was transferred to the chamber air through the aluminum end plates and also through the chamber doors opened briefly to uncap the hot-wire probe. This situation led to the development of a stratified air layer in the towing chamber. The results of the velocity runs performed during this stage gave a calibration curve that blended perfectly with the calibration curve desired in the wind tunnel. Before the flow conditions of the air in the chamber could be checked with "smoke," the temperatures inside and outside the chamber equalized and the calibration shift returned.

This occurrence provided evidence that a specific effect in the towing chamber was producing the observed calibration shift and that the effect was in some part affected by thermal stratification. It was surmised that if the air in the enclosed tow chamber was not stationary but in slight motion then the following would be observed: for a given velocity indicated by the rate of motion of the carriage, the actual velocity indicated by the hot-wire circuit would be equal to the mechanically induced velocity of the

probe plus the velocity of the airstream itself. The resultant combined velocity would be higher than the carriage speed if the tunnel air was in motion in a direction opposite to the motion of the carriage, and the resultant velocity would be less than the carriage velocity if the direction of motion of the airstream was in the same direction as the carriage. Such motions to the air in the towing chamber could be induced by the motion of the carriage and/or thermally through uneven temperature distributions in the chamber air, and they would be sensitive to stratification of the chamber air.

In order to maintain a degree of thermal stratification in the chamber air, the aluminum end plates were covered with $\frac{1}{2}$-inch Celotex insulating board. A series of calibrations was performed to determine the effect of the towing carriage and thermal stratification. Blocks of wood were added to the carriage bed to alter its length and/or height above the chamber floor. It was evident that these modifications were sufficient in themselves to produce a shift of the calibration curve. The magnitude and direction of the calibration curve translation depended upon the directional nature of the flow field in the chamber air set up by the particular carriage configuration. In the next step, dry ice was spread evenly over the chamber floor. This succeeded in forcing development of a cold layer of air sufficient in depth to engulf partially a modified carriage bed. The result was a shift in the calibration curve commensurate with an "effectively" less modified carriage bed. It was also demonstrated that with the original carriage bed and a stratified thermal situation, a probe mounted low in the chamber produced a "shifted" calibration curve while a probe mounted high in the chamber produced a calibration curve that was an extension of the wind tunnel curve.

On the basis of these results, the following conclusions were drawn: the calibration curve shift was due to the still air in the enclosed towing chamber starting in motion simultaneously with the start of movement of the carriage but with a resultant direction, at the probe, opposite to that of the carriage. When the aluminum plates were uninsulated, the air in the chamber was, temperature-wise, homogeneous owing to heat transfer inside the chamber with the outside ambient air through the aluminum end plates. Thus through procedure, the tests were being made only when the temperature in the chamber was homogeneous and the chamber air motion induced by the carriage motion were transmitted to the probe level. The air motion was contrary to the direction of motion of the carriage. This slight air velocity was added to the mechanical velocity of the hot-wire probe. The result was that the hot-wire bridge circuit measuring this resultant velocity required more current to balance than would be expected from mechanical velocity given through gears to the carriage. When the aluminum end plates were insulated, the temperature of the air in the chamber tended to stratify since it now lacked the heat transfer through the end

plates. As a result the motions of air set up by the motion of the carriage were damped below the level of the hot-wire probe and it was balanced with a current increase equivalent only to the mechanical velocity given, through gears, to the carriage.

It is felt that for future use the calibration towing chamber should be modified so as to eliminate the effects of air motions induced by the carriage bed without depending on the development of a stratified layer of cool air. The modifications would involve the streamlining of the carriage bed and/or the addition of a false floor and baffles to suppress induced chamber air motions.

Effect of Calibration on Wind Tunnel Velocity Profiles

In previous model smoke diffusion experiments reported,[3,5] all of the wind-tunnel velocity profiles were based on the assumption that the calibration curves for the hot-wire probes used followed a power law distribution from 0-8 fps. The work in the calibration towing chamber has produced an actual calibration curve for the probes that differs from a power law distribution particularly at speeds less than 1.0 fps. On this basis some of the low-speed results previously reported would have to be slightly revised. In previous experiments, however, there were only a few instances in which the air speeds determining the velocity profile were significantly less than 1.0 fps. Revisions in these data are not expected to alter any of the conclusions reported.

An example of the effect of the velocity probe calibration curve on a wind profile taken in the wind tunnel during the most recent series of tests (unreported) is as follows:

On the basis of the calibration curve given in Figure 28, a low-speed wind profile developed using profile plates in the wind tunnel, shown in Figure 30, for unstable temperature gradient ($dt/dZ = -0.70^\circ F/3.5$ ft.) would have an exponent of P = 0.22 where P is equal to $n/(2-n)$ and

$$\frac{u}{u_0} = \left(\frac{Z}{Z_0}\right)^{\frac{n}{2-n}}$$

If the speed values were interpreted from the straight extrapolation as given in Figures 27 and 28, the resultant wind profile shown in Figure 30, would have a P value of 0.29. From experience, the value of 0.22 would be the more representative value.

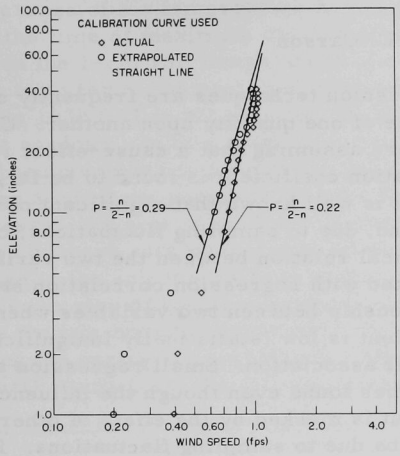

Figure 30

Wind profile for unstable thermal conditions ($dt/dZ = 0.7°F/3.5$ ft)

References

1. G. H. Strom and E. J. Kaplin. Calibration Towing Chamber. ANL Convective Turbulence Wind Tunnel Project, New York University Progress Report No. 504.03, Subcontract 31-109-38-743 (December 1961).

2. G. H. Strom and H. Moses. Model Smoke Diffusion Experiment, Argonne National Laboratory Radiological Physics Division Semi-annual Report. ANL-5829 (February 1958), pp. 211-217.

3. G. H. Strom and E. J. Kaplin. Convective Turbulence Wind Tunnel Project, Argonne National Laboratory Radiological Physics Division Semiannual Report. ANL-5967 (May 1959), pp. 195-209.

4. Weiss, R. F. Atmospheric Boundary Layer Simulation Techniques for Smoke Diffusion Experiments. Argonne National Laboratory Radiological Physics Division Semiannual Report. ANL-6104 (December 1959), pp. 116-124.

5. G. H. Strom and E. J. Kaplin. Convective Turbulence Wind Tunnel Project. Argonne National Laboratory Radiological Physics Division Semiannual Report. ANL-6199 (May 1960), pp. 119-132.

MULTIPLE REGRESSION ANALYSIS OF SOIL TEMPERATURE DATA

James E. Carson

Linear correlation and regression techniques are frequently used to estimate the degree of dependence of one quantity upon another. Considerable caution must be used before assuming that a cause-effect relationship does exist when a correlation coefficient is found to be large (that is, statistically significant). It is well known that significant correlation coefficients are sometimes found, due to sampling fluctuations, chance, etc., when, in fact, there is no physical relation between the two variables. Another type of error often associated with regression correlation studies is to reject as insignificant a relationship between two variables when the computed linear correlation coefficient is low (statistically insignificant), even though there is a real but small association. Small regression and/or correlation coefficients are sometimes found even though the influence of one variable on the other is large but is masked by the effect of other, unstudied parameters; or they may be due to sampling fluctuations. For example, Siegenthaler[1] found that the linear correlation between soil temperature and sunshine in Central Germany in winter was negative. This surprising conclusion is a consequence of the correlation between clear skies and cold winter days and nights in that area.

It is possible to estimate the degree of association of one variable with another, independent of the effect of other variables, by means of multiple regression and correlation techniques. The partial regression coefficient indicates the amount of change in the dependent variable (e.g., the change of soil temperature during a given time interval) per unit change of one of the independent variables (e.g., sunshine or wind speed), while the effects of the other variables considered in the analysis remain constant. The square of the multiple correlation coefficient shows the fraction of the variance of the dependent variable which can be explained by its association with all of the independent variables used in the analysis. The partial correlation coefficient is a measure of the association of the dependent variable and one of the independent variables, eliminating the effect of the other independent variables considered. The square of the partial correlation coefficient measures the ratio of the reduction of the square of the standard error of estimate of the dependent variable (when this independent variable is added to the analysis) to the square of the standard error of estimate without this variable but including the other independent variables.

The dependent variable (the predictand) used in these analyses is the change of the soil temperature at 1 cm during a time interval of one hour. Figure 31 shows the diurnal cycle of one-hourly temperature change in the air and soil, based on monthly average, for four typical months in 1955: January, April, July, and October. This figure, plus

similar diagrams for the other months of the year for the three-year period used in this analysis (1953-1955), shows that the time of the maximum rate of increase of air temperature is variable and typically occurs early in the day; the time of maximum decline is near sunset. The time of maximum rise in the 1-cm soil temperature also varies from month to month and from one year to the next in a given month but usually occurs at approximately 1000 CST in all seasons; the time of maximum fall also comes about sundown. In this study, a series of multiple regression equations has been computed to predict the change in soil temperature at 1 cm during a one-hour period at or near the times of maximum increase and decrease. Six sets of multiple regression equations have been prepared. Three of these sets were prepared to predict the one-hour temperature change in the soil for the hour ending at 1000 CST, at or near the time of maximum rise of soil temperature at 1 cm. The first set, Study A, predicts the one-hour temperature change at 1 cm from 0900 CST to 1000 CST during the spring season (March - May); Study B for the summer (June - August); Study C for the fall (September - November).

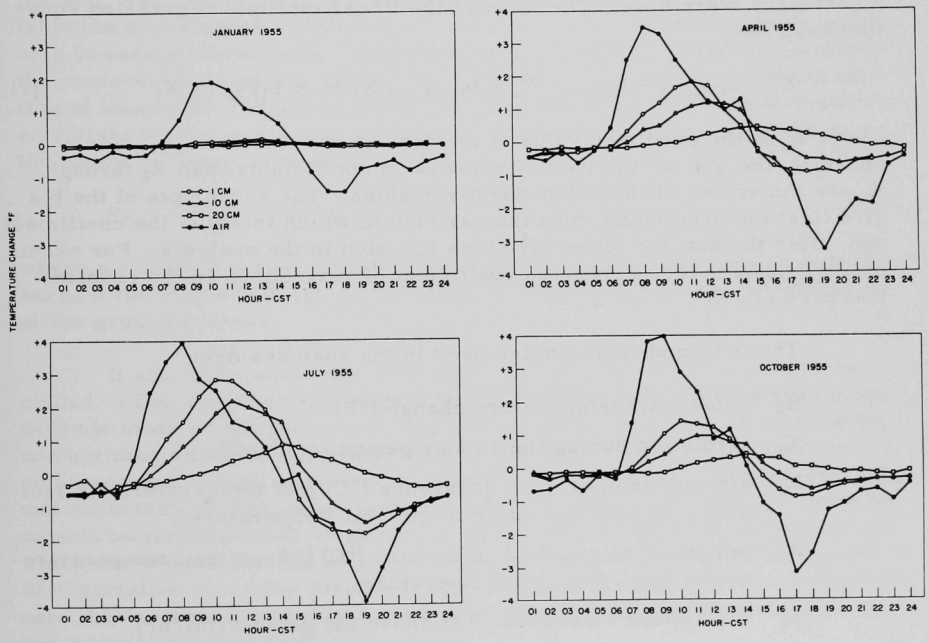

Figure 31

The average one-hour temperature changes in air and soil for the hourly period ending at the indicated time.

The remaining three sets of equations deal with conditions late in the afternoon. In Study D, the dependent variable is the change of the 1-cm soil temperature from 1600 to 1700 CST in the spring months; Study E, the change during the one-hour period ending at 1800 CST in summer; Study F for the hour ending at 1700 CST in the fall season. Because of difficulties involved in handling situations where the soil moisture changes phase and/or when there is a snow cover, no analysis of the data for the winter months was attempted. The 1-cm soil temperature is measured by means of a resistance thermometer in an area covered with pasture grass which is mowed periodically during the growing season. Details of the site and the measuring system used to collect and record the meteorological data used in this report may be found in previous reports[2,3] and will not be repeated here.

Any temperature change in the soil is the resultant of all the processes adding or removing heat from the soil at this level. Eight independent variables (the predictors), each of which is related to a heat-transfer mechanism, were used. The form of the linear multiple regression equation used is

$$X_1' = a_{1.23\ldots9} + b_{12.3\ldots9}\, X_2 + b_{13.24\ldots9}\, X_3 + \ldots + b_{19.23\ldots8}\, X_9 \quad , \qquad (1)$$

where X_1' is the predicted value of the dependent variable, $a_{1.23\ldots9}$ is a constant, the $\underline{b}$'s are the partial regression coefficients, and X_2 through X_9 are the values of the independent variables. The subscripts of the $\underline{b}$'s give first the predictand, then the variable of which this $\underline{b}$ is the coefficient, and, after the dot, the other variables included in the analysis. For example, $b_{14.2356789}$ is the regression coefficient of variable X_4 in the equation that predicts X_1'.

The independent variables used in the analyses are:

X_2 1-hour air temperature change (°F),

X_3 insolation during the 1-hour period (cal/cm^2),

X_4 air-soil temperature difference (°C) [air temperature 5.5 feet above surface minus the 1-cm soil temperature],

X_5 temperature gradient in the soil (°C) [10-cm soil temperature minus the 1-cm soil temperature],

X_6 wind speed measured 19 ft above the ground (mi/hr),

X_7 square root of vapor pressure in the air (mb),

X_8 the 1-cm soil temperature (absolute degrees) raised to the 4th power [(°A)^4],

X_9 atmospheric lapse rate (°C) [temperature difference between the 144- and 5.5-foot levels].

Variables 1 and 2 are the changes of soil and air temperatures during the hour ending at the times listed above; variable X_3 is the amount of sunshine during the same hour. The remaining variables (3 through 9) are the values measured on the hour at the start of the time intervals used in X_1, X_2 and X_3. Variable 2 reflects both the amount of sensible heat advected into the area during the hour and the amount of solar energy added to the air after being converted at the soil surface. It is obvious that X_1 and X_2 should be highly correlated. Variable X_3, the amount of sunshine reaching a unit horizontal area, is the amount of solar energy arriving at the air-soil interface and then reflected and converted into sensible and latent heat at the soil surface. Variables 4, 6 and 9 are all important factors controlling the convective transport of heat energy through the atmosphere. The temperature difference between the air and soil indicates the direction and, to a lesser extent, the magnitude of the heat transfer between the two media. The wind speed and temperature lapse rate are factors which, in part, determine the ability of the atmosphere to transport heat to or away from the surface. The temperature gradient in the soil, variable 5, is a measure of the amount of heat conducted to or from the soil surface to the deeper soil levels. This heat source or sink acts in such a direction as to prevent rapid changes of temperature near the surface. Variables 7 and 8 are important parameters controlling the flux of long-wave radiation to and from the soil surface. Typical of the empirical formulae for computing net radiation with cloudless skies is the following, suggested by Brunt (1939):

$$R_n = \sigma T^4 (1 - a - b\sqrt{e}) \quad , \tag{2}$$

where a = 0.44, b = 0.08, e is the vapor pressure at shelter height in millibars, σ the Stefan-Boltzmann constant, and T is the absolute temperature of the ground surface.

It should be noted that no index of the evaporative heat flux is included. (The vapor pressure term is not such an index since evaporation depends more on the difference in vapor pressure between the soil water and air than on the atmospheric vapor pressure itself.) No measure of soil moisture, which is also an important factor in the thermal conductivity and diffusivity of soil, was available. The effect of variable soil moisture on soil temperature can be somewhat reduced by using only those days on which no rain fell during a 48-hour period ending at the time of the dependent variable, X_1. This procedure reduces but, of course, does not eliminate the variable effect of changing soil moisture on evaporation and on the thermal properties of soil.

The actual calculations were done on the IBM 650 computer using a program prepared by Mr. M. J. Scherer of Data Processing Group, Argonne. The output of this program includes the following:

(a) the means and standard deviations of each variable;

(b) the linear simple correlation coefficients between each pair of the variables;

(c) the standard error of estimate of the regression equation,

$$S_{1.23...9} = \sqrt{\frac{\left[X_{1(calc)} - X_{1(obs)}\right]^2}{N - 9}} \qquad (3)$$

(d) the unbiased estimate of the multiple correlation coefficient, $R_{1.23...9}$;

(e) the partial regression coefficients, the a's and b's of Equation 1;

(f) the standard errors of the regression coefficients;

(g) the partial correlation coefficients between each pair of variables.

Twenty-four multiple regression computations were made. The first set of four equations, Study A, used the data for the three spring months of March, April and May. One regression equation for each of the three years of available data (1953, 1954, 1955) was calculated, as well as one equation using all of the data for the three years. Similar time periods were used for the five other studies. A complete description of the method of computation used has been given by Ostle.(4)

Table 10 lists the simple correlation coefficient between each pair of variables from Study C for the fall months using all three years of data. These data are based on 179 sets of data. The standard method for testing the significance of correlation coefficients was used.(4) These data reveal that all variables except X_6 are significantly related to the dependent variable. Not unexpected is the fact that sunshine intensity has the highest correlation with X. An interesting feature is the large correlation between the dependent variables and the net radiation terms (X_7 and X_8). The most surprising features of the table are the small correlation of wind speed (X_6) and the other eight variables and the smaller-than-expected coefficient between air- and soil-temperature changes, X_1 and X_2. The largest coefficient in the table, between X_7 and X_8, is a consequence of the increasing water-holding capacity of air as the temperature rises.

Table 11 lists the partial correlation coefficients between each pair of variables for the same analysis. It is interesting to note that the simple correlation between X_1 and X_7 was large and positive while the partial correlation coefficient, which is a measure of the interaction of the two terms when the effect of the other variables is held constant, is now negative. Variable 6 is now significant at the 5% level, while variable 5 no longer is. A surprising feature of this calculation is the relatively low correlation between the temperature changes in air and soil. Wind speed is now significantly correlated with five variables, while the correlations between sunshine and air- and soil-temperature changes are greatly reduced.

An examination of the data in Table 12 shows that the regression equation for the fall season yields a more accurate fit than for the other two seasons. The data also show that the equations are usually better for predicting the temperature changes in the afternoon than in the morning of a given season.

Table 13 shows the partial regression coefficients obtained in Study E using the data for each year and for all three years combined. Considerable variation was found in a given regression coefficient from one year to the next. If the procedures of statistics, based on random samples of independent data, are valid for these data, then the ratio

$$\frac{\sigma_b - \beta}{\sigma_b} \quad , \tag{4}$$

where β is the population parameter and σ_b is the standard error of the regression coefficient, is distributed as Student's t with (N-k) degrees of freedom. This test has been applied to the data in Tables 13 and 14 for $\beta = 0$.

Table 13

Partial regression coefficients for predicting the change of 1-cm soil temperature during the summer months for the hour ending at 1800 CST. (Study E)

	1953	1954	1955	3 years
Constant	2.59	8.33	8.96	8.29
$b_{12.3\ldots9}$	0.202*	0.211**	0.109**	0.125**
$b_{13.24\ldots9}$	-0.0068	-0.0088	-0.0002	-0.0059
$b_{14.}$	0.100	0.023	0.007	0.061**
$b_{15.}$	0.387*	0.183	0.109	0.170
$b_{16.}$	-0.052*	-0.072**	-0.049**	-0.049**
$b_{17.}$	0.423	0.742**	0.696**	0.708**
$b_{18.}$	-0.064	-0.157**	-0.159**	-0.151**
$b_{19.2\ldots8}$	-0.243	0.548*	-0.015	-0.014

*Coefficient significant at the 5% level.

**Coefficient significant at the 1% level.

Only two of the variables in this study (air-temperature change and wind speed) were found to be significant in all four sets of data. Sunshine is the only regression coefficient not significant in at least one of the four equations. An examination of this coefficient in the other two studies for predicting the temperature change near sundown (Studies D and F) is negative in all cases but one (1953 in the fall season). This is not unexpected

since the sunshine intensity at this hour is too small to prevent a rapid drop in air and soil temperatures under clear sky conditions. Under cloudy conditions, when the temperature falls at this time of day are small because of radiation from the clouds, insolation is near zero. Thus, negative correlations between sunshine and temperature changes are produced.

Table 14

Partial regression coefficients for predicting the 1-hour change of soil temperature at 1 cm

Study period	A 1954	A 1955	B 3 years	C 3 years	D 3 years	E 3 years	F 3 years
Hour ending	1000 CST	1000 CST	1000 CST	1000 CST	1700 CST	1800 CST	1700 CST
Constant	-8.81	-4.80	-0.56	-4.74	5.27	8.29	5.58
Variable							
X_2	0.194	0.072	0.169*	0.155**	0.147**	0.125**	0.168**
X_3	0.023**	0.021**	0.040**	0.025**	-0.017	-0.006	0.006
X_4	0.127**	0.049*	-0.052	0.105**	0.047*	0.061**	-0.014
X_5	-0.381*	-0.750**	-0.577**	-0.254	0.358**	0.170**	0.096
X_6	0.021	0.017	-0.023	-0.040**	-0.026	-0.049**	0.013
X_7	-0.635*	-0.283	-0.211	-0.524*	0.207	0.708**	0.768**
X_8	0.154**	0.077*	0.006	0.096	-0.087**	-0.151**	-0.128**
X_9	-0.611	-0.511*	-0.760**	-1.370**	0.709**	-0.014	0.236*
Sample size	55	67	194	179	143	183	177

*Coefficient significant at the 5% level.

**Coefficient significant at the 1% level.

There are several unexpected details in Table 13, however. For example, lapse rate is positively (and significantly) correlated with the dependent variable in 1954, but is negatively (although below the level of significance) related in the other three sets of data. Variable 4, the air-soil difference, is significant at the 1% level when all the data are combined, but it is not significant even at the 5% level in any given year.

An examination of similar tables for the other sets of data show that this pattern of fluctuating signs, magnitudes and degrees of significance of a given regression coefficient from one year to the next is typical. The relatively small sample size is a contributing factor in the instability of the regression and partial correlation statistics.

Table 14 lists the partial regression coefficients for the equations to predict the soil-temperature change from the meteorological data. Except for Study A, the coefficients listed are based on all three years of data.

Only one independent variable (sunshine) is significant in all four equations for the morning temperature change. An unexpected detail is the fact that the air-temperature change is not a significant predictor

of the dependent variable in Study A, but is in Studies B and C. The negative sign for the lapse rate coefficient indicates that unstable conditions (and greater heat flux in the atmosphere) favor greater soil warming.

Two predictors are significant in all three equations for afternoon conditions, air-temperature change and 1-cm soil temperature. Sunshine is not significant in any study. The sign of the lapse rate coefficient indicates that the formation of an inversion inhibits the soil temperature fall, while that of the soil temperature term (X_8) indicates that warm soil at sunset favors a rapid drop in temperature.

The most conspicuous feature of the table is the instability of sign, magnitude and significance of an independent variable from one year to the next and from one study to the next. This instability reduces the usefulness of the equations in predicting soil temperature changes. Two procedures to improve the effectiveness of the equations are suggested: a larger sample size and better screening of the input data to insure more homogeneous soil conditions.

Since, in meteorological practice, the simplest and shortest predicting systems are the most useful, it is logical to ask how much improvement in the forecast is made by including more and more predictors. The square of a linear correlation coefficient indicates the amount of variance of one variable that can be explained by its association with the other; the square of a multiple correlation coefficient indicates the fraction of the variance of the dependent variable that can be explained by its association with all of the independent variables.

Listed in Table 15 for Studies A, B and C are the linear correlation coefficients between variables 1 and 3, the only variable whose regression coefficient is significant in all four equations.

Table 15

Linear and multiple correlation coefficients

Study period	A 1954	A 1955	B 3 years	C 3 years	D 3 years	E 3 years	F 3 years
r_{13}	0.625	0.667	0.517	0.712			
r^2_{13}	39%	44%	27%	51%			
r_{12}					0.213	0.411	0.420
r^2_{12}					5%	17%	18%
R	0.870	0.885	0.627	0.850	0.760	0.804	0.820
R^2	76%	78%	39%	72%	58%	64%	67%

Also shown in the table are the linear correlation coefficients between variables 1 and 2 for the afternoon studies. This pair of variables was significant in all three studies. The multiple correlation coefficients and the squares of the coefficients are included. It is observed that considerable improvement in the forecast is made by the inclusion of more predictors. The most unusual item of this table is that only 5% of the variance of soil temperature change in the spring months in the afternoon can be explained by the air-temperature change. The value of the linear correlation coefficient between the one-hour temperature changes in air and soil (0.712) in Study C indicates that 51% of the variance in the soil can be explained by its relation to the temperature change in air. The multiple correlation coefficient for the same period (0.850) shows that 72% of the variance of X_1 can be explained by the eight independent variables. Thus, the seven additional variables improve the accuracy of the forecast by 19%.

References

1. J. Siegenthaler. Bodentemperaturen in Abhängigkeit von ausseren meteorologischen Faktoren. Gerlands Beitr. Geophys., 40 305-332 (1933).

2. J. E. Carson. Soil temperature and weather conditions. Argonne National Laboratory Report ANL-6470 (1961).

3. H. Moses and J. H. Willett. Five-year climatological summary, July 1949-June 1954. Argonne National Laboratory Report ANL-5592 (1957)

4. B. Ostle. Statistics in Research. Ames, Iowa: Iowa State University Press, 1954.

5. H. A. Panofsky and G. W. Brier. 1958: Some applications of statistics to meteorology. University Park, Penn.: Pennsylvania State University Press, 1958.

PUBLICATIONS

July 1961 to April 1962

Anderson, W. R., and I. B. Berlman. Radiant Flux from a Cylindrical Distributed Source. J. Opt. Soc. Am. 51 1229-1234 (1961).

Carson, James. E. Soil Temperature and Weather Conditions. Argonne National Laboratory Report ANL-6470 (Nov. 1961).

Failla, P. In Vivo and In Vitro Recovery of Irradiated Gametes of Arbacia Punctulata. Biol. Bull. 121 374 (1961). Abstract.

Machta, L., and H. F. Lucas. Radon in the Upper Atmosphere. Science 135 296-299 (1962).

Marinelli, L. D., C. E. Miller and H. F. Lucas, Jr. The Retention of Radium in Humans from 20 to 29 Years after Intravenous Administration and Some of Its Physiological Implications. Radiology 78 544-552 (April 1962)

Marshall, J. H. Microscopic Metabolism of Calcium in Bone. Bone as a Tissue, ed. K. Rodahl, J. T. Nicholson and E. M. Brown, New York: McGraw-Hill Book Co., 1960. pp. 144-155.

May, H. A., and L. D. Marinelli. Sodium Iodide Systems: Optimum Crystal Dimensions and Origin of Background. Proc. IAEA Symp. on Whole Body Counting, Vienna, June 12-16, 1961. Vienna: Intern. Atomic Energy Agency, 1962. pp. 15-36.

Miller, C. E., and L. D. Marinelli. Retention of Radium in Humans from 20 to 29 Years After Intravenous Administration. Proc. IAEA Symp. on Whole Body Counting, Vienna, June 12-16, 1961. Vienna: Intern. Atomic Energy Agency, 1962. pp. 279-284.

Miller, C. E. An Experimental Evaluation of Multiple-Crystal Arrays and Single Crystal Techniques. Proc. IAEA Symp. on Whole Body Counting, IAEA, Vienna, June 12-16, 1961. Vienna: Intern. Atomic Energy Agency, 1962, pp. 81-120. Also abstracted in Health Phys. 6 238 (1961).

Remenchik, Alexander P., and C. E. Miller. The Measurement of Total Body Potassium in Man and Its Relation to Gross Body Composition. Proc. IAEA Symp. on Whole Body Counting, Vienna, June 12-16, 1961, Vienna: Intern. Atomic Energy Agency, 1962. pp. 331-339.

Moses, H., and H. Daubek. Errors in Wind Measurements Associated with Tower-Mounted Anemometers. Bull. Am. Meteorol. Soc. 42 190-194 (1961).

Moses, H., and G. Strom. A Comparison of Observed Plume Rises with Values Obtained from Well-Known Formulas. J. Air Pollution Control Assoc. 11 455-466 (1961).

Gill, G. C., H. Moses, and M. E. Smith. Current Thinking on Meteorological Instrumentation for Use in Air Pollution Problems. J. Air Pollution Control Assoc. 11 77-82 (1961).

Moses, H., and F. Kulhanek. Argonne Automatic Meteorological Data Processing System. J. Appl. Meteorol. 1 69-80 (March 1962).

Durup, J., and R. L. Platzman. Role of the Auger Effect in the Displacement of Atoms in Solids by Ionizing Radiation. Discussions Faraday Soc. 31 156-166 (1961).

Wasko, P., and H. Moses. Photogrammetric Technique for Studying Atmospheric Diffusion. Photogrammetric Engr. 27 92-98 (1961).

PAPERS SUBMITTED FOR PUBLICATION

Anderson, R. W., and P. F. Gustafson. The Retention of Cesium-137 in Human Rib Bone. Science

Berlman, I. B. A Study of the α/β Ratio in a Liquid Organic Scintillation Solution. Intern. Congr. on Radiation Research, Harrogate, England, Aug. 6-10, 1962. Abstract.

Di Ferrante, Elvira. Studies on Ra^{226}, Po^{210} and Th^{228} in Bovine Bones and Teeth.

Lucas, H. F., D. E. Wallace, A. F. Stehney and F. H. Ilcewicz. Correlation of the Ra^{228} and Ra^{226} Content of Man with That of the Food and Water of His Environment. Intern. Congr. on Radiation Research, Harrogate, England, Aug. 6-10, 1962. Abstract.

Marinelli, L. D., and H. F. Lucas, Jr. The Translocation of Thorium Daughters to the Skeleton of Thorotrast Patients. 10th Intern. Congr. of Radiology, Montreal, Canada, Aug. 26-Sept. 1, 1962. Abstract.

Hasterlik, R. J., C. E. Miller and A. J. Finkel. The Late Effects of Radium Deposition in Humans. Intern. Congr. on Radiation Research, Harrogate, England, Aug. 6-10, 1962. Abstract.

Finkel, A. J., and C. E. Miller. Patterns of Radium Retention in Mice as Related to Man. Intern. Congr. on Radiation Research, Harrogate, England, Aug. 6-10, 1962. Abstract.

Moses, H., H. F. Lucas, Jr., and G. A. Zerbe. The Effect of Meteorological Variables Upon Radon Concentration Three Feet Above the Ground. J. Air Pollution Control Assoc.

Platzman, R. L. Dissociative Attachment of Subexcitation Electrons in Liquid Water and the Origin of Radiolytic "Molecular" Hydrogen. Intern. Congr. on Radiation Research, Harrogate, England, Aug. 6-10, 1962. Abstract.

Jesse, W. P., and R. L. Platzman. An Isotope Effect in the Probability of Ionizing a Molecule by Energy Transfer from a Metabolic Noble-gas Atom.

Rowland, R. E. High Resolution Autoradiographic and Microradiographic Studies of Bone and Teeth from Human Radium Cases. 10th Intern. Congr. of Radiology, Montreal, Canada. Aug. 26-Sept. 1, 1962. Abstract.

Wald, Neil, C. E. Miller, W. M. Borgas, and J. Kim. A Cytogenic Study of Some Radium Dial-Painters and Their Progeny. Intern. Congr. on Radiation Research, Harrogate, England, Aug. 6-10, 1962. Abstract

PAPERS ACCEPTED FOR PUBLICATION

Anderson, W. R., and I. B. Berlman. A Study of the Radiant Flux Output from a Cell Containing a Radiation-Damaged Scintillating Solution. Nucleonics.

Berlman, I. B., and A. Weinreb. On the Fluorescence Spectrum and Decay Time of Naphthalene. Mol. Phys.

Berlman, I. B. Ultraviolet and Lifetime Studies of Mechanisms in the Scintillation Process. Conference on Luminescence, New York University, Oct. 9-13, 1961.

Chhabra, Amrik S. Sr^{90}-Y^{90} Beta-Ray (and Bremsstrahlung) Depth Dose Measurements in Lucite. Radiology.

Frenzen, Paul. On the Origin of Certain Scintillation Patterns of Atmospheric Diffusion. Tellus.

Holtzman, R. B. The Desirability of Expressing Concentrations of Mineral-Seeking Constituents of Bone as a Function of Ash Weight. Health Phys.

Marinelli, L. D. Dosimetrie. Chapter III-1, Handbook of Medical Radiology Vol. 15, No. 11. Heidelberg: Springer-Verlag.

Marinelli, L. D., and H. F. Lucas. Translocation of Thorium Daughters to Bone. Proc. Symp. on Some Aspects of Internal Irradiation, Heber, Utah, May 8-11, 1961. Pergamon Press; also in Proc. the Bioassay and Analytical Chemistry 7th Annual Meeting, Argonne National Laboratory, October 1961. To be published as an ANL report.

Marinelli, L. D., C. E. Miller and H. F. Lucas, Jr. The Retention of Radium in Humans from 20 to 29 Years after Intravenous Administration and Some of Its Physiological Implications. Radiology.

Marinelli, L. D., C. E. Miller, H. A. May and J. E. Rose. Low Level Gamma-Ray Spectrometry: Experimental Requirements and Biomedical Applications. Advances in Biological and Medical Physics, Vol VIII. New York: Academic Press.

Marshall, J. H. Radioactive Hotspots, Bone Growth, and Bone Cancer: Self-Burial of Calcium-Like Hotspots. Counc. Intern. Organ. Med. Sci., Symp. on Radioactive Isotopes and Bone, Princeton, N. J., August 28-Sept. 3, 1960. Springfield: C. C. Thomas.

Platzman, R. L. Superexcited States of Molecules and the Primary Action of Ionizing Radiation. The Vortex.

Rowland, R. E. Skeletal Retention of the Alkaline Earth Radioisotopes and Bone Dosimetry. Proc. Symp. on Some Aspects of Internal Irradiation, Heber, Utah, May 8-11, 1961. Pergamon Press.